ISSN 0742-0463, Journal of Volcanology and Seismology, 2007, Vol. 1, No. 6, pp. 372–396. © Pleiades Publishing, Ltd., 2007.
Original Russian Text © I.S. Chuvashova, S.V. Rasskazov, T.A. Yasnygina, E.V. Saranina, N.N. Fefelov, 2007, published in Vulkanologiya i Seismologiya, 2007, No. 6, pp. 19–45.

Holocene Volcanism in Central Mongolia and Northeast China: Asynchronous Decompressional and Fluid Melting of the Mantle

I. S. Chuvashova, S. V. Rasskazov, T. A. Yasnygina, E. V. Saranina, and N. N. Fefelov

Institute of the Earth's Crust, Siberian Branch, Russian Academy of Sciences, Irkutsk, 664033 Russia

Received December 25, 2006

Abstract—Volcanic eruptions in central Mongolia during the latest Pleistocene and Holocene time preceded an initial Holocene volcanic event of 8740 ± 400 years ago in Northeast China and terminated simultaneously with that event as inferred from ^{14}C datings. Alkali basaltoid magmatic material from a partially melted (1.5–3%) mantle source was erupted in the Taryat Basin of central Mongolia, at first along a nearly east–west line of volcanoes, and afterwards material of higher melting (up to 5%) was discharged along the north–northeast line of Khorgo edifices. A material of similar composition was erupted in the Jingpohu area, Northeast China during the period from 5430–4400 BP. Initial liquids of ~2% beneath the Frog Pool volcanic center and ~5% beneath Crater Forest were expressed varying liquids beneath the latter area, yielding final melts of ~5%. The action of the decompressional and the fluid mechanism was followed by in eruptions of, respectively, isotope-homogeneous magmas in central Mongolia and isotope-heterogeneous magmas depleted in high field strength elements (Nb, Ta, Ti) in Northeast China.

DOI: 10.1134/S0742046307060024

INTRODUCTION

The causes of the Cenozoic tectonic activation in Central and East Asia are a subject of debate. The occurrence of Cenozoic volcanism in the Baikal region and Mongolia has been explained by the existence of sublithospheric sources of deep hot material [23, etc.]. The India–Asia collision has been invoked as initiating the generation of magma [7, etc.]. When the whole of Central and East Asia was under consideration, hypotheses were suggested as to the existence of a large convective flow or smaller plumes generated at the core–mantle boundary [3, 14, 26, 46, 54, and later publications].

The high-resolution upper mantle shear velocity model derived from surface wave data by T.B. Yanovskaya and V.M. Kozhevnikov [55] revealed the depth-dependent character of Cenozoic upper-mantle evolution in Asia. The Transbaikalian low-velocity domain has been identified in the 350–200 km depth range, with the Sayany–Mongolia, Sea-of-Okhotsk, and Philippine Sea low-velocity domains being confined to the 200–50 km range. The origin of the Transbaikalian low-velocity domain was related to Mesozoic–Cenozoic subduction of oceanic plates under East Asia, while the Sayany–Mongolia domain was thought to have been due to the India–Asia collision affecting Central Asia [18, 20, 48].

An earlier analysis of trace element partition in Cenozoic volcanic rocks sampled in central Mongolia and east China showed that that rocks from these areas did not have any compositions that could characterize a lithospheric mantle modified by subduction (with a high Ba/Nb) or a MORB-type source (basalts of mid-oceanic ridges with lower Nb/Y and higher Zr/Y) [27]. However, all geochemical parameters of Cenozoic volcanic rocks in these areas are not identical. Isotope ratios for Pb, Nd, and Sr establish the depleted isotope composition of the general component of the sublithospheric convective common in East Asia relative to the general sublithospheric component in Central Asia. This bias was considered as an indicator of the extent to which the depleted oceanic material that was subducted beneath Asia was involved in magma generation [19]. Identification of features peculiar to the magma generation spatially related to the Transbaikalian and Sayany–Mongolia low-velocity domains seems to call for more discriminating comparative studies.

We have conducted comparative investigations of the age and composition of the youngest volcanic rocks in central Mongolia (the Taryat Basin) and Northeast China (Jingpohu and Wudalianchi). Geochronometric data on volcanic eruptions in the Udokan and Changbaishan ranges were used to study age correlations between volcanic processes occurring in distant areas. The ranges contain differentiated series from alkali basalts to trachytes (up to pantellerites in the Changbaishan Range). Such series are absent from the volcanic fields in the Taryat Basin and the Jingpohu and Wudalianchi regions, so their compositions have not been considered.

The Holocene volcanic area in the Taryat Basin characterizes the processes in the central part of the Sayany–Mongolia low-velocity mantle domain, the Udokan range spatially corresponds to the northwestern part of the Transbaikalian low-velocity domain, and

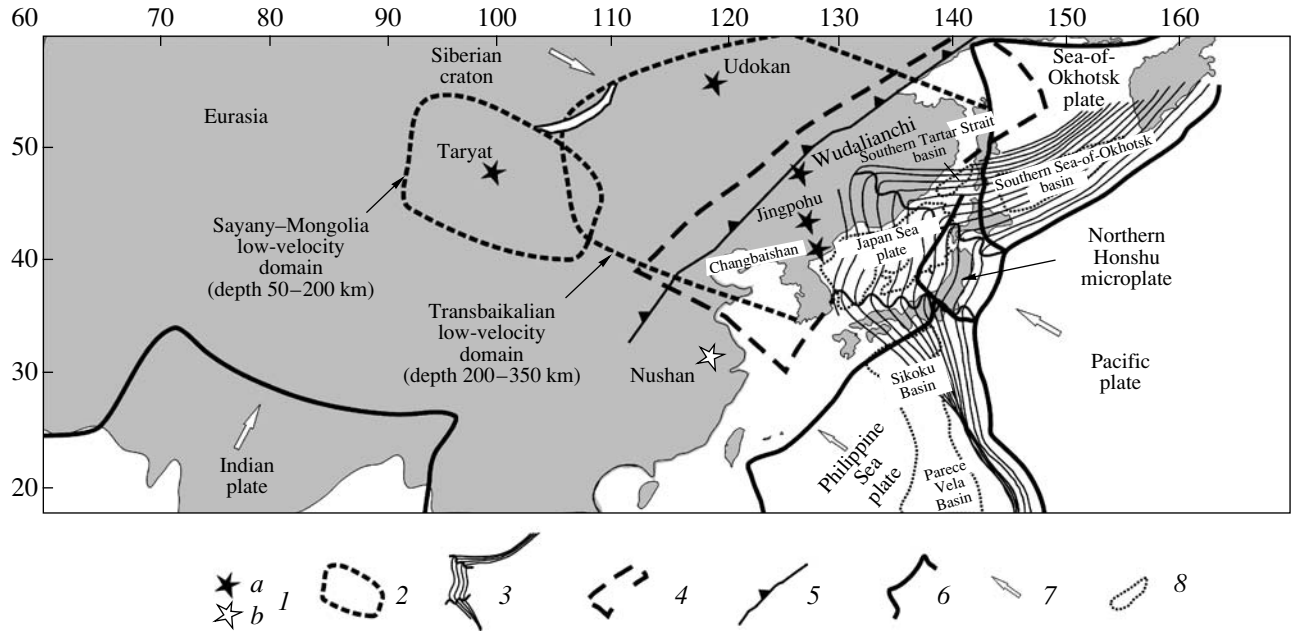

Fig. 1. Positions of the areas of Holocene volcanism in Eurasia considered in this paper: (*1*) areas of volcanic activity Latest Pleistocene and Holocene, (*2*) outlines of low-velocity domains [18], (*3*) active Pacific slab (the depth outline of the top of the dipping seismic zone is shown by isolines at intervals of 50 km [36]) together with the Hokkaido–Amur flexure coinciding with the direction of convergence between the Pacific plate and Eurasia, and with the Japan–Korea flexure oriented at an angle of 20° to the direction of convergence, (*4*) stagnant slab of transitional mantle zone [48], (*5*) border gravity step [22], (*6*) variant of plate boundaries modified from [62], the boundary of the northern Honshu plate being shown after [50], (*7*) present direction of plate motion, (*8*) deep-sea backarc basin produced by strong Cenozoic extension (spreading).

areas in northeast China correspond to its southeastern part. The latter are situated in the frontal part of the active Pacific slab subducting beneath Eurasia. The slab belongs to the central part of the high-velocity anomaly in the mantle transition zone (depths of 410–660 km), known as a "stagnanting slab" [34]. The northwest outline of the high-velocity anomaly is advanced inland relative to the border gravity step of East Asia by approximately 300 km. The Wudalianchi region is immediately to the east of the border gravity step, and the Jingpohu and Changbaishan regions are farther toward the continental margin (Fig. 1).

The effects of plate convergence on intraplate processes may be felt both in the crustal stress and strain and in modifications of deep magma compositions. The change in crustal stress and strain can be inferred from the structural rearrangement of the volcanic zone, with its magma conduits being spatially reoriented and its volcanic centers rearranged. The fact that this rearrangement temporally coincided with the change in deep magma composition reflects the action of tectonic processes in the mantle, as well as in the crust. The goal of the present study is to determine the evolution of deep-seated magmatic processes during the short time interval of Holocene volcanism in central Mongolia and northeast China.

THE DATA

Characterization of the volcanism. Volcanic activity in the Taryat Basin has resumed periodically since the Late Miocene [10, 12, 24, 28]. Holocene lavas obstructed a wide valley to produce Lake Terkhiin-Tsagan-Nur. The eruptions were concentrated in a zone about 4 km long. Its western part contains the Odnobokii, Listvennichnyi, and Sosnovyi volcanoes aligned in a nearly east–west row. The eastern part of this zone contains the north–northeast line of Khorgo Volcano edifices (Fig. 2). Yu.S. Genshaft and A.Ya. Saltykovskii [1] show these volcanoes as an arcuate chain.

Odnobokii Volcano occupies the westernmost place in the east–west volcanic line. A volcanic explosion affected the mountain slope with a crescent-shaped crater lip 400 m long adjacent to it. The lip is composed of bombs and large blocks of porous basalt. The next edifice, Listvennichnyi Volcano, is flooded by lavas, with only the top being exposed. The crater is about 1 km in diameter with a visible height of the crater lip of up to 60 m. The crater was filled with lava flows, which became extrusive–effusive domes a few tens to a few hundred meters across. The third volcano, Sosnovyi, is flooded by lavas to a still greater extent. Its crater has a diameter of ~700–800 m with a visible crater lip height within 30 m. The crater lip is composed of red, occasionally pumice-like lapilli and infrequent large (up to 2 m) basalt bombs. The crater is filled with small lava flows and domes. The amount of pyroclastic material

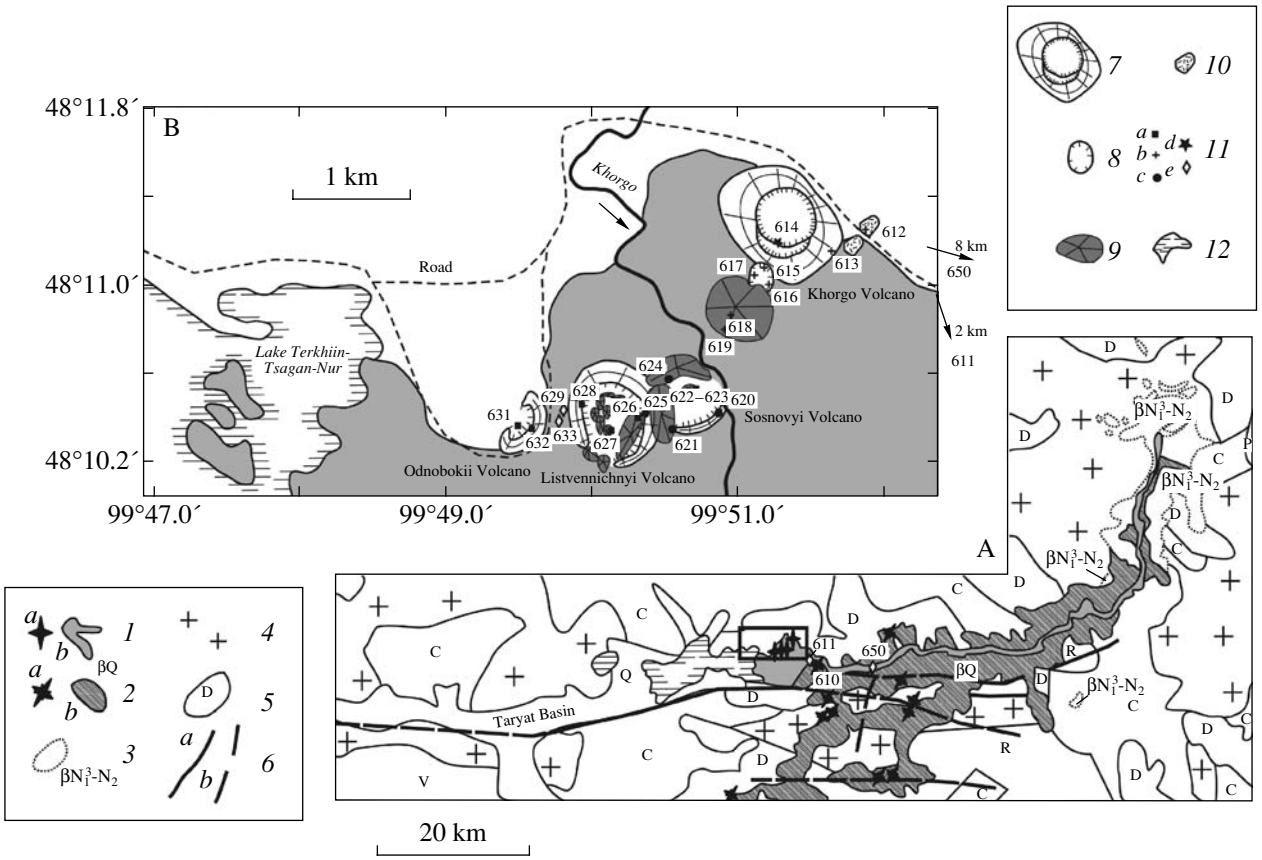

Fig. 2. Geological setting for Holocene volcanism in central Mongolia: (A) overall distribution of Late Cenozoic volcanic rocks in the Taryat Basin, (B) distribution of Holocene volcanic edifices. (*1–6*) (legend for A): (*1*) Holocene volcanoes (*a*) and associated flows (*b*), (*2*) Pleistocene volcanoes (*a*) and associated flows (*b*), (*3*) volcanic rocks of Late Miocene to Pliocene (βN_1^3–N_2), (*4*) Permian granitoids, (*5*) sedimentary complexes (age indices run from Riphean (R) to Carboniferous (C), (*6*) faults, (*a*) reliable and (*b*) uncertain; (*7–11*) (legend for B): (*7*) volcanic cone with summit crater, (*8*) lateral crater, (*9*) lava dome, (*10*) loose fan of pumice-like cinder and volcanic bombs, (*11*) sites of rock sampling, numbers corresponding to those in Table 1, in the east–west line of volcanoes (*a* basanite–phonobasanites, *b* phonobasanite–phoidites), in the Khorgo line (*c* basanite–phonobasanites, *d* basaltic trachyandesites), and in the lava flows that had formed the dam in the basin (*e* basanite–phonobasanites), symbols corresponding to those in Fig. 5, (*12*) major lakes. Panel A is based on map materials found in [1, 2, 6, 8, 12].

decreases and that of the lava increases as one moves from Odnobokii to Listvennichnyi.

The edifices of the Listvennichnyi and Sosnovyi volcanoes are surrounded by a lava plane complicated with sags that formed after the lava tunnels were emptied. The sags are as deep as a few tens of meters, the depth may reach 15 m. The lava flows have well-preserved surfaces. When found around the volcanoes, they mostly have smooth or slightly undulating surfaces with sparse vegetation.

The Khorgo volcanic cone has a diameter of 1200 m at the base, a height of 120 m, its slope dips at 45° or more steeply, and the crater has a diameter of 180 m and a depth of 70 m. The cone is composed of cinders, agglutinates, and bombs. Some bombs are as large as 6 m across. No lava is found within the crater. The crater walls are nearly vertical at the top. A loose fan of pumice-like cinder formed near the eastern and northeastern base of the cone with the inclusion of volcanic bombs as large as 1 m across. A lateral crater that has been cut into the southwestern edge of the Khorgo volcanic cone is partially filled with lava. A few large bombs have rolled down into the lateral crater from the slope of the central volcanic cone. Near the lateral crater is a lava dome, some of which has propagated onto the crater slope. The central slope, the lateral crater, and the lava dome had a common feeding conduit striking north–northeast (azimuth 30°).

The Khorgo lava flows are highly porous and have an irregular blocky surface produced by flowing volatile-rich lava breaking through and collapsing its top. There is no vegetation on the surface of the lava flows, except some at the edges.

The Jingpohu Holocene volcanic zone is one of a nearly north–south chain of volcanic fields about 350 km long where eruptions have repeatedly resumed since the Eocene. The Holocene eruptions were preceded by eruptions of Pleistocene volcanic centers in the time

interval 1.2–0.9 Ma, these latter being controlled by northeast faults [41]. The Holocene eruptions were concentrated in a nearly north–south Crater Forest line 16 km long and at the Frog Pool volcanic center. The latter is situated 13 km northeast of crater no. 1, which marks the northern termination of the Crater Forest line (Fig. 3).

The Wudalianchi region is notable for the potassium composition of its lavas. This region is in the central part of a nearly north–south chain of volcanic fields approximately 140 km long. Apart from the Wudalianchi field, there are two more volcanic fields, Erkeshan and Keluo, which have potassium compositions. The Wudalianchi and Keluo fields contain 14 volcanic cones each, the Erkeshan field has two twin volcanoes. The Wudalianchi and Erkeshan fields formed during the last 2 Ma, while the Keluo field has Late Miocene lavas, in addition to Quaternary ones [52, 58].

Correlations of volcanic eruptions by ^{14}C datings. The Late Pleistocene and Holocene volcanism in the Udokan Range, northern Transbaikalia is well understood geochronometrically [15 and the references therein], and for this reason the area is the standard for comparisons when studying the evolution of Holocene volcanism in Central and East Asia.

The terminal volcanic activity in the Udokan Range occurred in an arcuate east–west zone of Quaternary volcanism 20 km long. Alkali–olivine–basalt–hawaiite melts were discharged at the ends of the zone, while mugearite, benmoreite, and trachyte melts were erupted in the central part. The earliest pyroclastic material of the Trakhitovyi Volcano has been ^{14}C dated using woody remains at 12050 ± 650 years. When calibrated to the year 1950, the calendar date was 14400 ± 1600 years (here and below, all calendar dates are assigned at the mid-points of confidence intervals, with the calculations being performed by the Calib Rev 5.1 beta program, using an IntCa104 calibration curve [49]). Later, biotite trachytes were erupted by Dolinnyi Volcano 8780 ± 260 years ago, by Aku Volcano 5310 ± 270 years ago, and by Chepe Volcano approximately 2200 years ago. The last event was determined as the mean of three calendar dates with a probability greater than 95%. Alkali-basaltic lavas were erupted by Syni Volcano approximately 9800 years ago (the figure is the mean of four calendar dates, each with a probability greater than 94%).

The calendar dates for the alkali-basaltic Syni Volcano and the trachyte Dolinnyi Volcano have overlapping confidence intervals and are combined into a single volcanic episode occurring 9800–8780 years ago. The Dolinnyi eruption was notable for a high explosivity index and the discharge of fine-grained trachyte pumice occasionally saturated with oval inclusions of partially crystallized basic material. Such an eruption may have been triggered by a sudden release of volatile components due to decompression, provoked by emplacement of an alkali-basaltic melt into a shallow trachyte magma chamber. The 9800–8780 BP volcanic episode is generally interpreted as an episode of contrasting alkali-basaltic and trachyte volcanism [19].

The volcanoes that were active from 14400–9800 BP were controlled by a northwest fault, and the Dolinnyi Volcano, together with the volcanoes that erupted after it, was controlled by a northeast fault. The state of crustal stress and strain changed by the end of the contrasting magmatism episode, i.e., about 8780 BP.

The upper time limit for the discharge of lava flows in the Taryat Basin is found from ^{14}C datings of organic matter sampled in the lacustrine sediments that overlie the lavas: 4930 ± 150 BP [12] and 6890 ± 400 BP [2]. The respective calendar dates are 5690 ± 260 and 7710 ± 810 BP. The volcanic eruptions themselves have not been dated. Their timing is estimated by assuming that the rearrangement of Holocene volcanic zones in the Taryat Basin and in the Udokan Range occurred simultaneously. The lower time limit for the Khorgo eruption and the discharges of lava flows that have flooded the area (see below) is taken to be the eruption time for the Dolinnyi Volcano, with that eruption marking the structural rearrangement of the Udokan volcanic zone 8780 ± 260 BP. It thus appears that the eruption of the Khorgo Volcano and its lava flows must be confined within the interval 8780–7710 BP. The timing of the eruptions on the east–west volcanic line in the Taryat Basin is similar to that of the earlier eruptions in the Udokan Range during the time interval 14400–9800 BP.

Forty-four volcanic events are to be found in the literature for Northeast China based on archival records of historical eruptions and ^{14}C datings. The earliest Holocene eruption of trachyte pumice by Bingchang Volcano in southern Jilin Province was characterized by a ^{14}C dating of 7854 ± 180 BP [57]. The calendar date of that eruption, 8740 ± 400 BP, is identical to the date 8780 ± 400 BP for the Dolinnyi Volcano, which also was erupting trachyte lava in the Udokan Range. The beginning of Holocene volcanism in Northeast China was contemporaneous with the structural rearrangement of the Udokan volcanic zone (Fig. 4).

Eruptions occurred at the Jingo, Frog Pool, and Changbaishan volcanoes and the Crater Forest in the interval 5910–4400 BP. The ^{14}C date for the first of these volcanoes is 5140 BP [59] (a calendar age of 5910 years). The Crater Forest line in the Jingpohu region has three ^{14}C datings: 4630 ± 60 BP for crater I at the northern end of the line and 3950 ± 70 and 3970 ± 70 BP for crater V in the central part of the line. A ^{14}C date of 4460 ± 80 BP was obtained for the Frog Pool volcanic center [61]. The calendar dates of the eruptions are 5380 ± 110, 4400 ± 180, 4430 ± 200, and 5430 ± 160 BP, respectively. The activity time of the Frog Pool volcanic center is comparable with that for the eruption at crater I, Crater Forest line, within the measurement uncertainty. The Jingpohu volcanism is considered to have proceeded in three eruption cycles.

The first and second cycles took place both in the Crater Forest line and at the Frog Pool volcanic center, while the third was confined to activity on the Forest line [61]. A date of 4105 ± 90 BP was obtained for the Changbaishan Volcano [44] (the calendar age is 4630 ± 210). In the latter case it was the trachyte pumice that accumulated north of Tianchi Crater that was dated. The interval of activity on volcanoes of Northeast China 5910–4400 BP is to be compared with the eruption of the trachyte Aku volcano in the Udokan Range whose calendar date is 5310 ± 270 BP.

Later eruptions at Changbaishan Volcano have been characterized by 22 ^{14}C datings within the total range 2420 ± 95 to 910 ± 45 BP [44] (the range of calendar dates is 2530 ± 220 to 830 ± 90 BP). There is a record of historical eruptions on Changbaishan, with the last dating back to 1903. A magma chamber that exists today at a depth of 15–25 km beneath Tianchi Crater was identified by electromagnetic soundings and studies of S-wave velocity variations.

The beginning of frequent activity on Changbaishan was approximately simultaneous with an eruption on the Chepe Volcano in the Udokan Range (~2200 BP). In addition to similar trachyte compositions of ejecta thrown out by Holocene volcanoes in Northeast China and in the Udokan Range, one also notices the approximately simultaneous resumption of volcanic activity in these regions since 7780–7740 BP. One difference occurred from 2500–2200 BP, when the Udokan volcanism terminated with the Chepe eruption, while Changbaishan entered a phase of frequent eruptions.

The last volcanoes to erupt in the Wudalianchi region were Laoheishan and Huoshaoshan. Data contained in historical Manchu archives show that the former became active on January 14, 1720, and ceased erupting before the end of March 1721, while the latter began erupting April 26 and ceased in June 1721 [44].

Volcanic rock composition. The abundances of major oxides in the volcanic rocks of the Taryat Basin have been briefly reviewed by V.V. Kepezhinskas et al. [8] and by other workers. The localities of the samples examined were not, however, specified, so that our study in "young" volcanism has to restrict itself to samples from a new collection only. The sampling sites on the volcanoes are shown in Fig. 2, with the coordinates measured by the GPS device being listed in Table 1.

The volcanic rocks of Holocene volcanoes belong to a Quaternary volcanic complex of mostly basanite–phonobasanite composition with less abundant basaltic trachyandesites and phonobasanite–phoidites. A special marker of the lava succession is provided by basaltic trachyandesites with K–Ar datings of 1.9 Ma [9, 32, an unpublished K–Ar dating of ours]. Rocks of this composition are also found in higher parts of the section dated 1.3–1.2 Ma [10, 24]. The phonobasanite–phoidite group mostly belongs to the terminal phases of Quaternary volcanism. The Holocene volcanoes show a wide compositional range, from phonobasanite–phoidites to basaltic trachyandesites (Figs. 5a, 5b).

The rocks found in the east–west line of the Odnobokii, Listvennichnyi, and Sosnovyi volcanoes are for the most part comparable in their contents of major oxides with the volcanic rocks in the Khorgo line. The difference consists in higher-alkali phonobasanite–phoidites on the Sosnovyi and Listvennichnyi volcanoes, while the crater of the Khorgo volcanic cone contains relatively lower-alkali basaltic trachyandesites. The total alkali content and K_2O/Na_2O decrease together with increasing SiO_2. Compared with older Quaternary basaltic trachyandesites, a rock of the same composition in the Khorgo crater has a low K_2O/Na_2O. The lavas sampled from flows within 10 km of the Holocene volcanoes are all in the basanite–phonobasanite group.

Figure 6 shows the distribution in volcanic rocks of incompatible trace elements Ba and Zr in relation to the magnesium number Mg# = Mg/(Mg + Fe^{2+}) (with the correction $Fe^{3+} = 0.15\ Fe_{total}$, u).

The values of the Mg# are generally higher in the basanite–phonobasanite group than in phonobasanite–phoidites and basaltic trachyandesites. The concentration of Ba in all three rock groups is 500–800 ppm. The concentration of Zr is generally lower in basaltic trachyandesites than in basanite-phonobasanites, and higher in phonobasanite–phoidites.

The variations in volcanic rock composition for the Jingpohu region are generally similar to those in the Taryat Basin (Figs. 5c, 5d, Table 2). In the alkali–silica classification diagram, the volcanic rocks of the Crater Forest line form a series from phoidites to trachybasalts, being somewhat shifted relative to the Taryat volcanic rocks (lower SiO_2). The Frog Pool phonobasanite–phoidite group is comparable with that found in the Taryat Basin. The K_2O/Na_2O ratio in the Jingpohu rocks varies in the range 0.47–0.80 (0.49–0.59 for trachybasalts) and overlaps the range of this ratio for the Taryat rocks. The magnesium number Mg# is increased (60.8–67.0) in the Crater Forest basanites, and decreases in the trachybasalts, down to the range 59.3–61.4, being as low as 47.1–49.1 in the Frog Pool phonobasanite–phoidites. As to the abundance of barium, the Jingpohu volcanic rocks are comparable with the Taryat rocks (Figs. 6c, 6d).

Fig. 3. Geological setting of Holocene volcanism in Northeast China. Panel A shows the overall distribution of Cenozoic volcanic rocks in the area of study, B and C are zones of Holocene volcanism in Wudalianchi and Jingpohu regions: (*1*) Cenozoic volcanic fields in A. For the other symbols see Fig. 2. Panel C shows pre-Quaternary volcanic rocks (Pliocene βN_2 and Eocene βE). The maps are based on [41, 52, 58, 61].

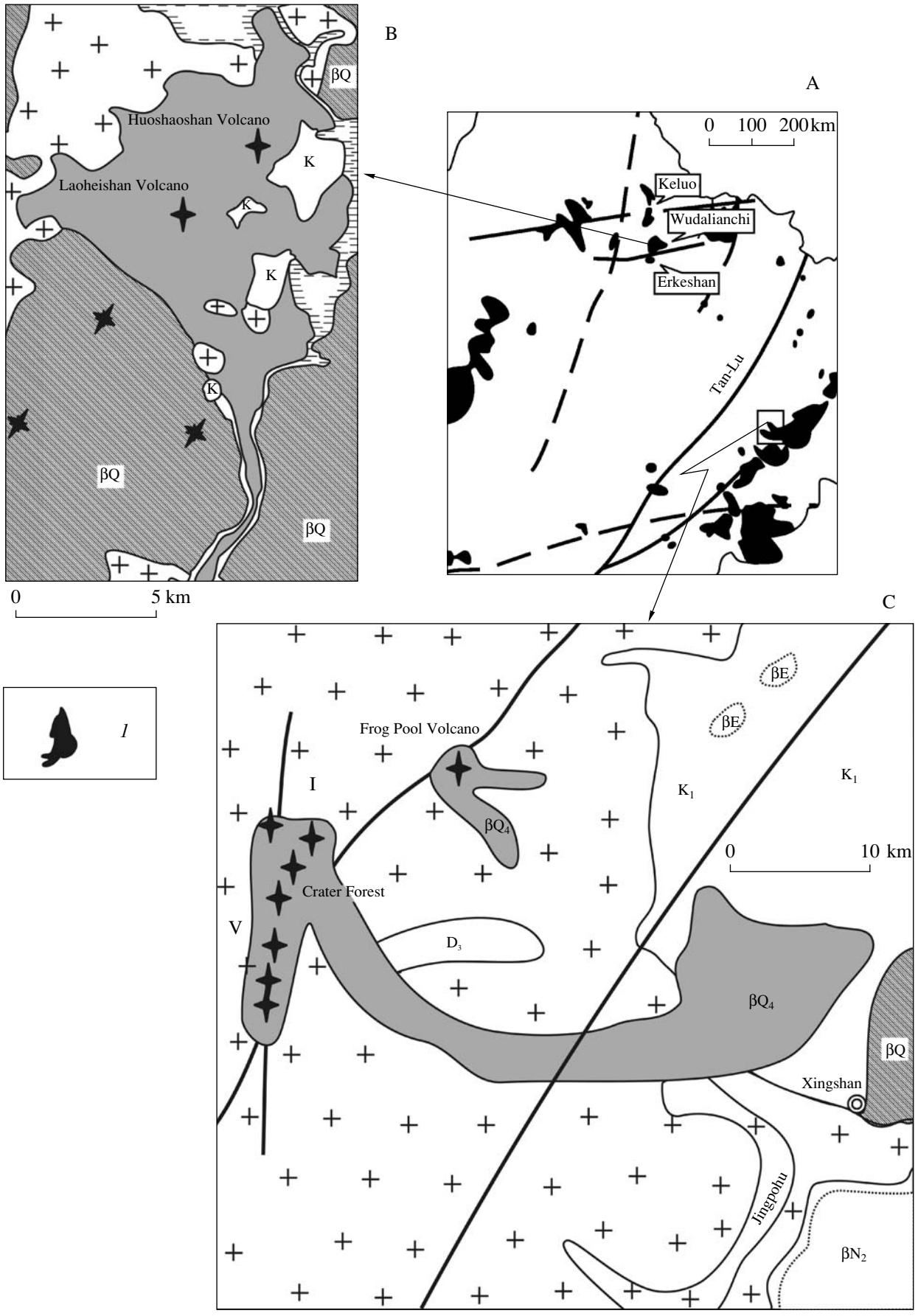
B
βQ
Huoshaoshan Volcano
K
Laoheishan Volcano
K
K
K
βQ
βQ
0
5 km
A
0 100 200 km
Keluo
Wudalianchi
Erkeshan
Tan-Lu
C
1
βE
βE
Frog Pool Volcano
I
K1
K1
βQ4
0
10 km
Crater Forest
V
D3
βQ4
βQ
Xingshan
Jingpohu
βN2

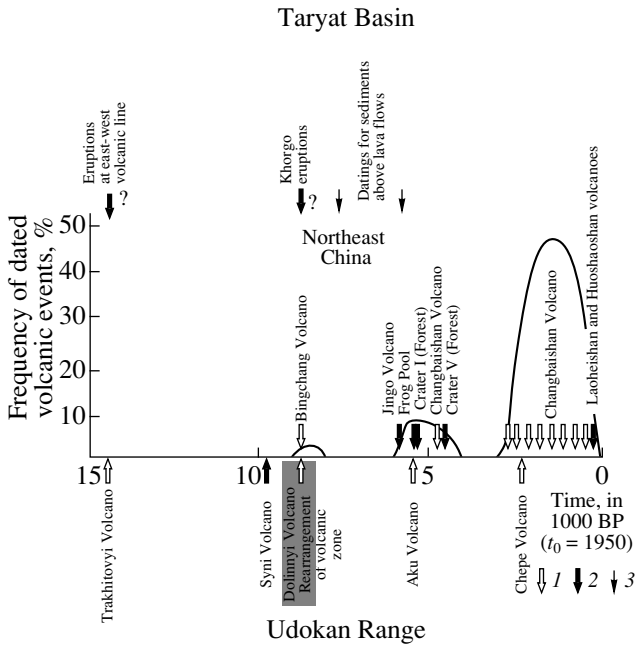

Fig. 4. The timing of volcanic eruptions in the Udokan Range compared with eruptions in the Taryat Basin and Northeast China: (*1–3*) calendar dates for trachyte (*1*) and alkali-basaltoid (*2*) eruptions and lacustrine sediments overlying the lavas (*3*). The question mark denotes hypothetical eruption times. The calendar dates are those converted from [2, 12, 15, 44, 57, 59, 61]. The diagram of eruption frequency for Northeast China (44 datings in all) was constructed using a moving window of 1000 years.

There are also several differences between the Jingpohu and the Taryat rocks, in particular, in the abundances of high field strength elements. The concentrations of Zr range between 200 and 380 ppm in the Taryat basanite–phonobasanites, and are 239 ppm in the Khorgo basaltic trachyandesite and 390–430 ppm in the phonobasanite–phoidites of the Sosnovyi and Listvennichnyi volcanoes (Fig. 6). The concentration of Zr in the Jingpohu rocks is relatively low, not above 252 ppm for Crater Forest and 345–349 ppm for the Frog Pool volcanic center. This last range of concentration is lower than that for the phonobasanite–phoidites of Sosnovyi and Listvennichnyi volcanoes. As Mg# decreases in the Crater Forest trachybasalt–phoidite series, the concentration of Zr somewhat decreases, reaching the lowest values in the trachybasalts (167–180 ppm). The content of TiO_2 varies in the range of 2.0 to 2.5 wt % in the Taryat volcanic rocks and 1.3 to 2.0 in the Jingpohu rocks. The lowest concentrations of Zr in trachybasalts are accompanied by the lowest concentrations of TiO_2 (Tables 1, 2). The figurative points for the Taryat volcanic rocks in the Th/Yb–Ta/Yb diagram (Fig. 7) are aligned along the mantle direction, while the points for the Jingpohu volcanic rocks lie higher.

The compositions of the Wudalianchi volcanic rocks exhibit several peculiar features (Figs. 5, 6). The Quaternary lavas of that area are enriched in SiO_2 (50–57 wt %). The points for the rocks of the present-day volcanoes Laoheishan and Huoshaoshan form an extended trend of gradually decreasing SiO_2 from 55 to 46 wt % with a narrow range of total alkali content, 8.5–9.5 wt %. Some of the Laoheishan and Huoshaoshan rocks, in the range 51–55 wt % for SiO_2 (marked as the Lh1 group in the figures), are comparable with the Wudalianchi Quaternary rocks in their range of K_2O/Na_2O (1.3–1.6), while some other rocks having lower concentrations of SiO_2, 47–50 wt % (marked as the Lh2 group) differ from these by a lower K_2O/Na_2O (1.1–1.2). The concentrations of the incompatible elements Ba and Rb are high in the Wudalianchi rocks. The concentrations of Zr in the Lh2 group are relatively low, but increase significantly in the Lh1 group, exceeding those in the Wudalianchi Quaternary rocks. The concentrations of TiO_2 are partly low (1.9–2.0 wt %) and partly increased (2.2–2.5 wt %). The highest concentrations of Zr (540–630 ppm) in the Lh1 rock group of Laoheishan and Huoshaoshan volcanoes are accompanied by low concentrations of TiO_2. The Th/Yb–Ta/Yb diagram (Fig. 7) shows the Wudalianchi volcanic rocks to be shifted above the mantle direction, similarly to the Jingpohu rocks.

DISCUSSION

Estimation of the degree of partial melting in mantle sources. This study on the mantle sources of central Mongolia and Northeast China was carried out by direct and inverse modeling of partial melting. In the direct modeling, the melt compositions were calculated based on assumed source composition and then compared with the compositions of volcanic rocks. The inverse modeling uses the same equations as direct modeling, but the passage was from source composition to trace element concentrations in real volcanic rocks.

The equation for equilibrium melting has the form [51]

$$C_i = \frac{C_i(0)}{D_i + F(1 - P_i)}, \quad (1)$$

where C_i is the concentration of element i in the melt, $C_i(0)$ is the same for source, D_i is the bulk partition coefficient, F the degree of partial melting, $P_i = \sum X^j K_i^j$ is a weighting factor for the liquid distribution, X^j is the fraction of the phase coming into the melt, and K_j is the partition coefficient for phase j.

The equation of fractional melting is somewhat different [51]:

$$C_i = \frac{C_i(0)}{D_i}\left(1 - \frac{P_i F}{D_i}\right)^{(1/P_i - 1)}. \quad (2)$$

Table 1. Concentrations of major oxides (wt %), trace elements (ppm), and strontium isotope ratios in the Taryat Latest Pleistocene and Holocene volcanic rocks of central Mongol

Column number	1	2	3	4	5	6	7	8
Specimen number	Mn-633	Mn-650	Mn-611	Mn-612pk	Mn-612pg	Mn-612	Mn-613	Mn-615
Lat. deg.	48°10.38′	48°8.98′	48°10.00′	48°11.21′	48°11.21′	48°11.21′	48°11.14′	48°11.65′
Long. deg.	99°49.8′	99°57.43′	99°53.31′	99°51.85′	99°51.85′	99°51.85′	99°51.66′	99°51.19′
SiO_2	48.67	48.78	47.83	47.58	47.75	48.20	48.16	49.79
TiO_2	2.04	2.14	2.32	2.28	2.20	2.19	2.24	2.13
Al_2O_3	14.15	14.91	14.88	14.69	14.57	14.92	14.03	14.65
Fe_2O_3	2.60	2.36	2.86	2.30	2.60	1.92	2.48	3.25
FeO	7.83	8.19	7.55	8.00	7.68	7.86	8.04	7.17
MnO	0.14	0.15	0.13	0.13	0.13	0.13	0.14	0.14
MgO	9.47	7.80	8.00	8.56	8.70	8.19	8.16	7.75
CaO	7.02	7.05	6.44	6.16	5.75	6.46	7.00	7.00
Na_2O	4.36	4.60	4.74	4.86	5.19	5.03	4.88	4.46
K_2O	2.80	3.10	4.02	3.89	4.03	3.97	3.52	2.68
P_2O_5	0.72	0.79	1.00	0.97	1.07	0.98	0.90	0.62
H_2O^-	0.10	0.16	0.12	0.16	0.13	0.14	0.14	0.19
H_2O^+	0.33	0.45	0.37	0.84	0.40	0.41	0.65	0.55
Total	100.23	100.48	100.26	100.42	100.20	100.40	100.34	100.38
Sc	16.9	14.7	14.1	12.1	11.3	10.9	14.6	14.1
Cr	363	212	297	226	241	230	227	195
Co	49	41	43	42	40	39	42	41
Ni	291	160	246	232	261	225	198	155
V	176	159	148	139	126	134	155	157
Cu	40	37	33	34	35	30	37	36
Zn	99	106	123	104	152	100	106	95
Rb	39	41	48	44	47	44	43	41
Sr	812	904	1124	1044	1136	1043	966	714
Y	20.0	19.7	20.3	18.9	20.7	19.8	20.3	18.5
Zr	233	301	352	324	350	332	332	198
Nb	53	59	73	66	73	67	62	45
Mo	7.2	3.2	4.2	4.8	5.1	4.7	4.7	2.9
Cs	0.40	0.53	0.45	0.44	0.64	0.41	0.40	0.43
Ba	518	642	618	579	735	603	540	530
La	41.1	48.5	63.7	59.3	67.8	59.5	53.0	32.2
Ce	82.3	94.6	121	113	171	115	103	66.4
Pr	9.2	10.3	13.5	12.6	14.1	13.0	11.8	7.54
Nd	37.5	42.3	52.0	47.7	54.9	48.8	44.4	31.4
Sm	7.60	8.14	9.52	9.56	10.0	9.37	8.27	6.85
Eu	2.32	2.60	2.90	2.76	2.95	2.95	2.64	2.24
Gd	6.18	6.78	7.66	7.76	8.16	7.70	6.86	6.03
Tb	0.93	0.96	1.05	0.99	1.10	1.07	0.99	0.81
Dy	4.59	4.53	5.28	4.73	5.28	4.94	4.77	4.41
Ho	0.79	0.74	0.77	0.74	0.81	0.81	0.80	0.72
Er	1.85	1.91	1.84	1.96	1.90	1.81	2.07	1.93
Tm	0.3	0.2	0.2	0.2	0.2	0.2	0.3	0.2
Yb	1.47	1.34	1.36	1.27	1.27	1.32	1.42	1.43
Lu	0.18	0.21	0.15	0.14	0.15	0.19	0.20	0.19
Hf	5.50	6.31	7.10	6.81	7.28	7.30	6.88	4.98
Ta	3.4	3.6	4.5	4.2	4.7	4.4	3.9	3.0
W	0.4	0.4	0.7	0.8	0.9	1.0	0.7	0.5
Pb	5.7	6.7	7.8	7.7	8.2	7.4	7.6	6.4
Th	4.90	5.13	6.15	6.13	6.49	6.05	5.50	4.41
U	1.29	1.40	1.67	1.68	1.67	1.63	1.55	1.25
$^{87}Sr/^{86}Sr$	0.704670 ± 14	Not dtm.	Not dtm.	Not dtm.	Not dtm.	Not dtm.	0.704697 ± 15	0.704795 ± 15

Table 1. (Contd.)

Column number	9	10	11	12	13	14	15	16
Specimen number	Mn-616	Mn-617	Mn-618	Mn-619	Mn-626	Mn-627	Mn-628	Mn-629
Lat. deg.	48°10.97′	48°11.1′	48°10.82′	48°10.59′	48°10.39′	48°10.35′	48°10.39′	48°10.38′
Long. deg.	99°51.19′	99°51.15′	99°51.11′	99°50.99′	99°50.33′	99°50.14′	99°50.00′	99°49.8′
SiO_2	48.12	49.55	48.80	48.74	47.90	47.42	47.53	49.84
TiO_2	2.07	2.13	2.20	2.14	2.35	2.32	2.23	2.21
Al_2O_3	14.29	14.49	14.95	14.40	14.57	14.45	14.80	15.05
Fe_2O_3	6.35	3.13	1.30	1.74	2.71	3.11	2.40	1.95
FeO	4.63	7.30	9.08	8.44	7.85	7.44	7.69	8.24
MnO	0.14	0.14	0.15	0.15	0.12	0.14	0.15	0.15
MgO	9.05	7.83	8.10	9.01	7.46	8.06	8.05	7.64
CaO	6.66	7.49	7.29	6.89	6.09	6.31	6.59	6.74
Na_2O	4.40	4.24	4.13	4.06	4.95	4.77	4.65	4.34
K_2O	3.10	2.62	2.61	2.95	4.30	4.08	4.26	2.96
P_2O_5	0.77	0.63	0.60	0.73	1.18	1.16	1.19	0.68
H_2O^-	0.20	0.09	0.02	0.03	0.09	0.28	0.10	0.03
H_2O^+	0.62	0.60	Not dct.	Not dct.	0.87	0.86	Not dct.	Not dct.
Total	100.40	100.24	99.65	99.88	100.44	100.40	100.24	100.30
Sc	13.8	16.4	15.7	18.9	10	12	9	19
Cr	300	192	Not dtm.	Not dtm.	199	241	Not dtm.	Not dtm.
Co	43	43	46	48	38	42	42	45
Ni	253	167	169	220	204	236	210	146
V	147	167	145	127	121	137	114	129
Cu	33	42	30	45	30	33	21	42
Zn	97	105	113	121	110	112	121	128
Rb	40	40	40	44	49	51	52	58
Sr	874	736	710	863	1306	1225	1296	923
Y	18.6	19.0	19.8	21.8	20.8	21.3	22.8	21.6
Zr	247	205	200	256	378	365	320	274
Nb	57	46	47	55	78	77	80	55
Mo	3.9	3.2	3.6	4.3	5.5	6.1	6.5	3.8
Cs	0.44	0.63	0.50	0.38	0.49	0.45	0.55	0.69
Ba	507	802	543	514	606	626	681	760
La	46.0	32.3	28.1	39.2	77.7	73.5	67.3	36.2
Ce	90.3	65.3	56.9	76.3	195	174	129	73.1
Pr	9.85	7.69	6.83	8.85	16.3	15.2	14.6	8.25
Nd	39.5	31.6	28.9	35.2	60.6	58.5	57.4	32.9
Sm	7.67	6.52	6.26	7.29	10.7	10.6	11.6	7.02
Eu	2.42	2.15	1.77	2.40	3.40	3.18	2.98	2.43
Gd	6.53	5.58	4.98	6.14	8.54	8.64	7.68	5.76
Tb	0.95	0.82	0.87	0.89	1.16	1.13	1.10	0.90
Dy	4.47	4.07	4.01	3.97	5.71	5.31	5.64	4.49
Ho	0.73	0.71	0.67	0.71	0.79	0.79	0.80	0.76
Er	1.86	1.75	1.61	1.62	1.93	2.06	1.76	1.70
Tm	0.2	0.3	0.2	0.2	0.2	0.2	0.2	0.2
Yb	1.48	1.43	1.47	1.32	1.15	1.21	1.36	1.60
Lu	0.18	0.22	0.18	0.18	0.16	0.14	0.14	0.17
Hf	6.09	5.11	4.90	4.84	7.59	7.08	7.32	5.38
Ta	3.8	2.9	2.9	2.6	4.9	4.7	4.9	2.8
W	0.6	0.4	0.6	0.5	1.0	0.8	1.2	0.4
Pb	7.1	6.1	5.4	5.7	8.8	8.4	7.0	7.2
Th	5.02	4.19	4.05	3.68	7.09	6.42	6.57	4.41
U	1.39	1.26	1.15	1.02	1.73	1.78	1.75	1.17
$^{87}Sr/^{86}Sr$	Not dtm.	Not dtm.	Not dtm.	Not dtm.	Not dtm.	Not dtm.	Not dtm.	Not dtm.

Table 1. (Contd.)

Column number	17	18	19	20	21	22
Specimen number	Mn-631	Mn-632	Mn-621	Mn-624	Mn-625	Mn-614
Lat. deg.	48°10.36′	48°10.4′	48°10.35′	48°10.35′	48°10.40′	48°11.15′
Long. deg.	99°49.51′	99°49.55′	99°50.51′	99°50.51′	99°50.38′	99°51.28′
SiO_2	48.36	48.32	47.59	48.43	48.26	50.51
TiO_2	2.18	2.21	2.29	2.32	2.32	2.11
Al_2O_3	14.88	14.95	15.48	15.50	15.71	15.23
Fe_2O_3	2.88	2.31	3.03	2.29	2.91	3.16
FeO	7.45	7.78	6.93	7.60	7.30	6.92
MnO	0.14	0.15	0.13	0.15	0.13	0.13
MgO	7.24	7.17	4.94	5.18	4.86	7.43
CaO	6.41	6.14	7.84	6.16	5.97	6.85
Na_2O	4.88	4.92	5.14	5.32	5.54	4.55
K_2O	4.06	4.20	4.71	4.87	4.75	2.00
P_2O_5	1.13	1.15	1.18	1.25	1.24	0.70
H_2O^-	0.23	0.05	0.16	0.09	0.25	0.13
H_2O^+	0.50	Not dct.	0.87	Not dct.	0.84	0.45
Total	100.34	99.87	100.29	99.70	100.08	100.17
Sc	12	13	8.6	7.4	7.8	15.4
Cr	217	ç.Ó.	84	Not dtm.	66	181
Co	39	39	32	35	32	42
Ni	202	146	82	86	80	158
V	134	97	112	99	106	165
Cu	33	33	29	28	32	39
Zn	123	127	123	138	131	98
Rb	48	53	54	58	54	44
Sr	1200	1292	1365	1412	1410	774
Y	22.0	24.0	21.8	22.9	21.5	21.9
Zr	366	360	432	414	392	239
Nb	77	77	90	92	90	55
Mo	4.7	6.7	6.0	7.0	5.8	3.8
Cs	0.66	0.46	0.54	0.56	0.54	0.49
Ba	773	605	608	673	591	587
La	72.0	70.1	77.2	71.9	78.7	38.6
Ce	180	133	195	135	149	78.8
Pr	15.2	15.1	16.4	15.1	16.4	8.9
Nd	57.4	55.2	63.4	61.9	64.9	36.4
Sm	11.1	10.8	11.5	11.3	12.2	7.85
Eu	3.28	3.46	3.51	3.09	3.57	2.23
Gd	8.82	8.31	9.04	8.36	8.48	6.84
Tb	1.19	1.06	1.18	1.21	1.13	0.96
Dy	5.30	5.53	5.37	5.30	5.10	5.00
Ho	0.78	0.80	0.79	0.81	0.77	0.86
Er	1.87	1.97	2.05	1.50	2.00	2.10
Tm	0.2	0.2	0.2	0.2	0.2	0.3
Yb	1.24	1.24	1.32	1.14	1.25	1.74
Lu	0.19	0.18	0.16	0.16	0.19	0.23
Hf	7.11	6.91	8.45	8.11	9.29	5.56

Table 1. (Contd.)

Column number	17	18	19	20	21	22
Specimen number	Mn-631	Mn-632	Mn-621	Mn-624	Mn-625	Mn-614
Lat. deg.	48°10.36′	48°10.4′	48°10.35′	48°10.35′	48°10.40′	48°11.15′
Long. deg.	99°49.51′	99°49.55′	99°50.51′	99°50.51′	99°50.38′	99°51.28′
Ta	4.7	4.2	5.6	5.4	5.6	3.5
W	0.8	0.7	0.9	1.3	1.0	0.6
Pb	9.0	8.2	9.0	8.1	9.5	7.0
Th	6.63	5.60	7.73	7.41	7.38	5.10
U	1.80	1.58	2.04	1.96	2.05	1.40
$^{87}Sr/^{86}Sr$	Not dtm.	Not dtm.	0.704722 ± 11	Not dtm.	0.704674 ± 12	0.704699 ± 12

Notes: 1–12, basanite–phonobasanites: 1–3, in lava flows, 4–12, at Khorgo line, 13–18, at the east–west volcanic line; 19–21, phonobasanite–phoidites at east–west volcanic line; 22, basaltic trachyandesite of Khorgo Volcano. Trace element composition was determined by inductively coupled plasma mass spectrometry with chemical preparation of samples by Chemical Analyst M.E. Markova using the technique described previously [25]. A specimen of 50 mg was put in a fluoroplastic container with a lid and a screwed-on cap, a 3 : 1 mixture of HF and HNO_3 was added, and then decomposed in a microwave furnace using hyperpure acids twice distilled and water distilled in the Elix-3 Millipore, France system. For complete elimination of silicon the specimen was twice evaporated with 1.5 ml HF and, after adding HNO_3, H_2O_2, and water, again evaporated. The measurements were made using a quadrupole VG Plasma Quad PQ 2+ mass spectrometer at the Baikal Analytical Center for Common Use. Two internal standards (In and Bi), were introduced into the specimen in order to correct for the influence of the matrix and time-dependent drift of the device. The correction for an element was obtained by interpolation. The analysis was checked by comparison with international standard specimens: BIR-1, BHVO-1, JB-2 (basalts), AGV-1 (andesite). The detection interval was between 0.005–0.009 ppm (Lu, Tb, Yb, Ho, Er) and 2–4 ppm (Ni, Zn, Sr, Ba). The specimens were decomposed in air in Teflon vessels by a mixture of concentrated hydrofluoric and nitric acids for determining strontium isotopes. Strontium was separated in single-use chromatographic columns using Sr. Spec, ELChrom Industries anion exchange resin using a technique with low consumption of reagents (HNO_3, H_2O). The Finnigan MAT 262 mass spectrometer at the Baikal Analytical Center for Common Use was used for isotopic analysis of strontium to determine strontium concentrations by isotopic dilution. During the measurement period, the values for the standard isotopic specimens of strontium were NBS SRM 987 0.710264 ± 0.000015 (a mean of two measurements), VNIIM 0.707992 ± 0.000020 (a mean of six measurements). The error in the measurement of strontium isotope ratios is shown by the last digits (2σ). Not dtm. means not determined, Not dct. means not detected.

Some manipulation of (1) yields the following relations for a strongly incompatible element H with $D_i \approx 0$ and $D_i \approx P_i$ [40]:

$$C_H/C_i = a_i C_i + b_i \quad (3)$$

$$a_i = D_i/C_i(0) \quad b_i = C_H(0)/C_i(0)(1 - P_i). \quad (4)$$

If volcanic rocks proceed from one and the same magma source, the trace element concentrations in them will obey (3). In order to pass from (3) to the bulk partition coefficients we use the relations [30, 53]

$$E = \frac{C_i(L)}{C_i(H)} = \frac{D_i + F(H)(1 - P_i)}{D_i + F(L)(1 - P_i)}, \quad (5)$$

where $F(H)$ is the highest degree of partial melting, $F(L)$ the lowest degree, and $C_i(H)$ and $C_i(L)$ are the respective concentrations of element i under these circumstances. For fractional melting we have

$$E = \frac{C_i(L)}{C_i(H)} = \frac{(1 - F(L))^{(1/D_i - 1)}}{(1 - F(H))^{(1/D_i - 1)}}. \quad (6)$$

We use La as a strongly incompatible element (in relation to undifferentiated mantle [45]). The degrees of partial melting, the highest $F(H)$ and the lowest $F(L)$, were first estimated from the $(La/Yb)_N$ vs. Yb_N relation. The next step was to calculate the bulk trace element partition coefficients from (5) and (6), assuming $D_i \approx P_i$ for the moment, and then to choose such a modal mineral composition of the source as to best fit D_i and P_i to the results of inverse modeling. The mineral/melt partition coefficients used here are listed in Table 3.

In rocks from Holocene volcanoes of central Mongolia for the range of 27 chemical elements, the C_{La}/C_i (Table 4) are directly proportional to C_{La}, with a high correlation coefficient (above 0.79; 0.62 for Ce). This shows that the magma melts were derived from the same mantle source region. The relatively lower correlation coefficient for Ni (0.79) may have been due to some distortion of the primary melt composition by crystallization differentiation of olivine. The relatively low correlation coefficient for Ce can be explained by its geochemical similarities with La. The correlation coefficients calculated for the sample of Quaternary volcanic rocks acquired in the Taryat Basin are practically indistinguishable from those of the rocks of Holocene volcanoes.

The bulk partition coefficients for modeled magma sources in central Mongolia are shown in Fig. 8. Direct modeling, which has been made to fit the results of

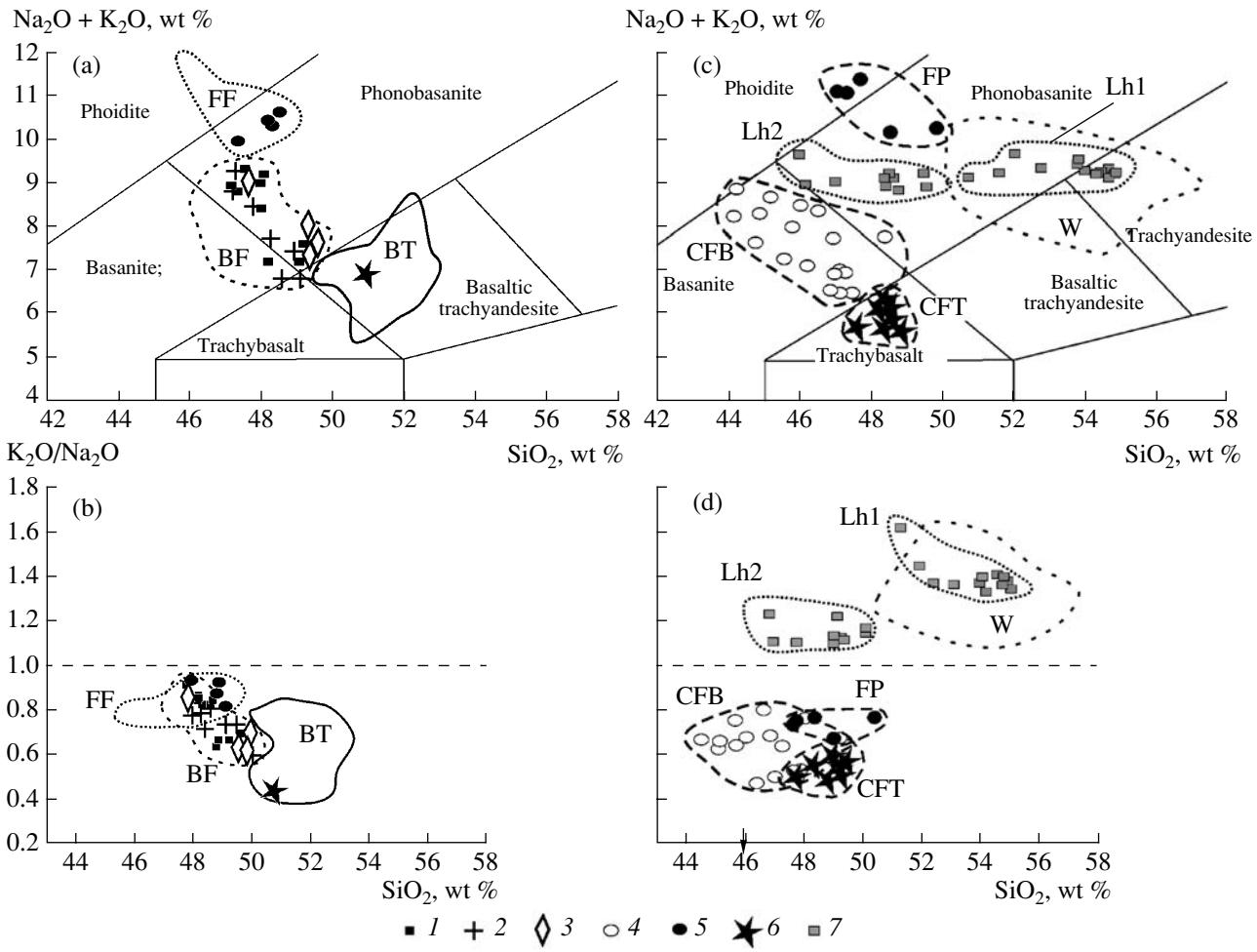

Fig. 5. The sum $Na_2O + K_2O$ and the K_2O/Na_2O ratio in relation to SiO_2 in volcanic rocks of central Mongolia (a, b) and Northeast China (c, d). (*1–3*) Rocks of Taryat volcanoes: (*1*) basanite–phonobasanite group from the east–west line of Odnobokii, Listvennichnyi, and Sosnovyi volcanoes, (*2*) same, Khorgo line, (*3*) same, lava flows surrounded by Holocene volcanoes, (*4*) Crater Forest basanites, Jingpohu region, (*5–6*) volcanic rocks of similar compositions in Taryat Basin and Jingpohu region: (*5*) phonobasanite–phoidite group of Sosnovyi, Listvennichnyi, and Frog Pool volcanoes, (*6*) basaltic trachyandesites and trachybasalts of Khorgo cone and Crater Forest, (*7*) potassium phonobasanite–trachyandesites of Laoheishan and Huoshaoshan volcanoes, 1720–1721 eruptions, similar in composition to earlier Wudalianchi Quaternary lavas (Lh1 group) and different from earlier Wudalianchi lavas in having lower K_2O/Na_2O and SiO_2 (Lh2 group). Diagrams a and b show highlighted figurative fields of Taryat Quaternary lavas (our unpublished data): basanite–phonobasanites (BF), phonobasanite–phoidites (FF), and basaltic trachyandesites (BT), diagrams c and d show highlighted groups of potassium phonobasanite–trachyandesites from the Wudalianchi, Erkeshan, and Keluo Quaternary volcanoes (W), Crater Forest trachybasalts (CFT) and basanites (CFB), Frog Pool phonobasanite–phoidites (FP). Data from [41, 52, 58, 61, 64] were used to construct c and d. Dividing lines are shown in a and c following the International Union of Geological Sciences. The compositions have been converted to 100%, ignition losses being subtracted

inverse modeling, revealed the composition of a metasomatized mantle source containing olivine (41%), orthopyroxene (20%), clinopyroxene (30%), garnet (5%), phlogopite (3.4%), ilmenite (0.5%), and apatite (0.1%). The trace element concentrations at the source were based on the composition of undifferentiated mantle [45] incorporating data on the average apatite composition from spinel lherzolites (type A) [47] and the phlogopites sampled from mantle xenoliths on Shavaryn-Tsaram Volcano, central Mongolia [42].

The results of direct modeling for the Taryat volcanic rocks are shown in the $(La/Yb)_N$–Yb_N coordinates (Fig. 9a). According to the equilibrium melting model, the phonobasanite–phoidites from Sosnovyi and Listvennichnyi volcanoes are interpreted as 1.5–2.0% partial melts. Some basanite–phonobasanite melts at the east–west line of volcanoes formed at a higher degree of melting, not above 3.0%, however. These low values of partial melting (1.0–1.7%) were calculated for rocks from the east–west line of edifices using the fractionation model.

The melts of the Khorgo line were derived from the same mantle source, but with higher degrees of melting (2–5% according to the model of partial melting, except for two points that fall in the interval 5–10%, and 1.5–4.0% according to the fractionation model). The basal-

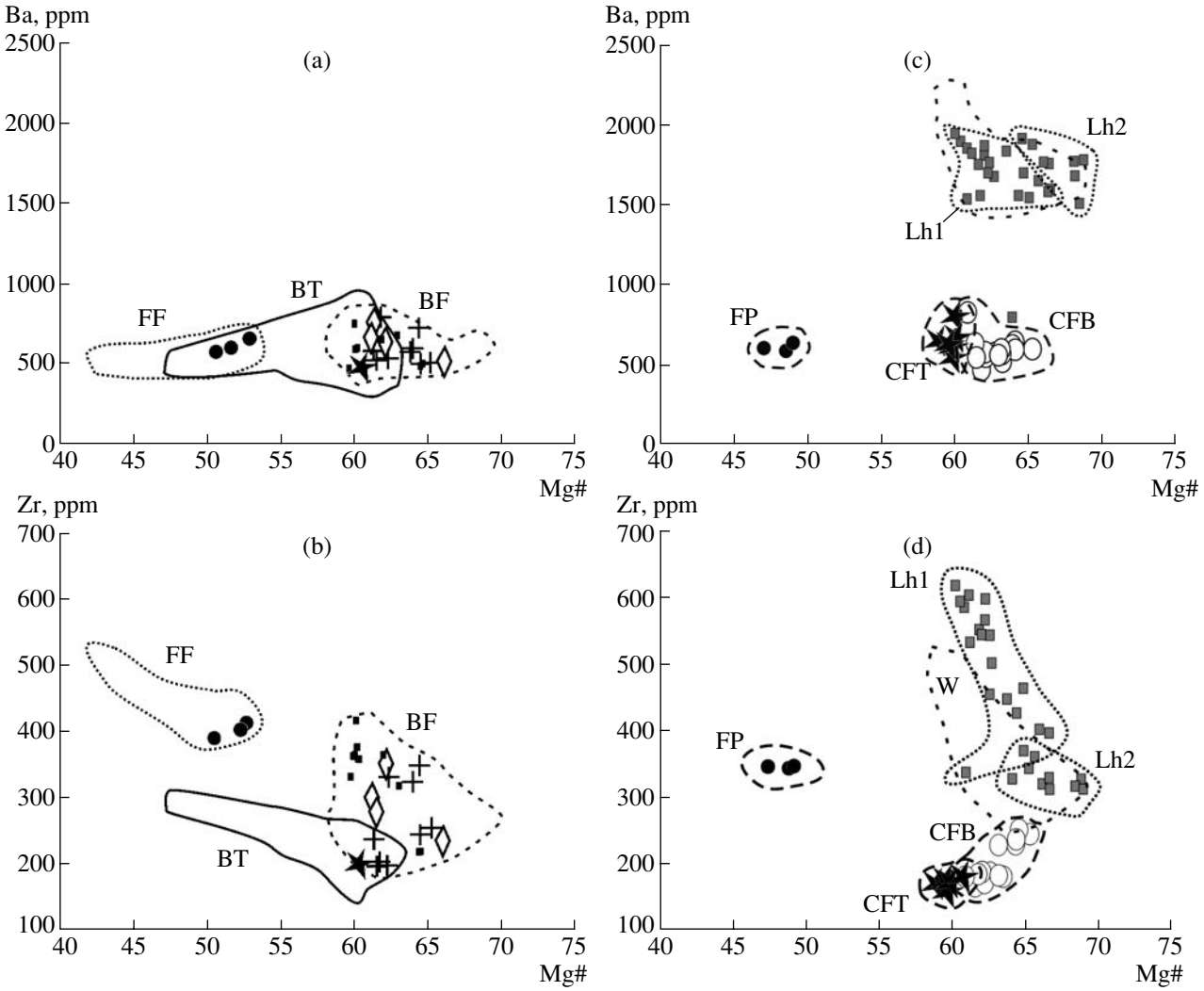

Fig. 6. Variations in Ba and Zr in relation to magnesium number Mg# in volcanic rocks of central Mongolia and Northeast China. For legend see Fig. 5.

tic trachyandesite of the Khorgo crater (sample MN-05-614) has higher ytterbium concentrations, which is interpreted as resulting from a decreased concentration of garnet in the mantle source, from 5 to 3%. The degree of melting at the mantle source that produced the lava flows around the volcanoes is comparable with the melting at the source of volcanic rocks for the Khorgo line.

Calculations by the partial-melting model using the concentrations of rare earth elements, as well as Nb, Ta, Ti, Zr, Hf, Rb, Ba, K, Th, U, Sr, Y, and Cr (Fig. 10), generally corroborate the results obtained in the $(La/Yb)_N$–Yb_N coordinates for the partial melting interval equal to 1.5–5%. However, the 5–10% degrees of partial melting are not reached for the concentrations of Th, U, Nb, and Ta. The offset of two points in the $(La/Yb)_N$ vs. Yb_N diagram (Fig. 9a) into the partial melting interval 5–10% can be explained by the complete depletion of garnet at the source with the highest degree of partial melting. When it is absent from the restite, the value of $(La/Yb)_N$ must dramatically decrease, approaching that for garnetless paragenesis.

In contrast to the volcanic rocks sampled in the Taryat Basin, the volcanic rocks in Northeast China show some slight correlation between most trace elements, so that inverse modeling does not yield reliable results for these. The most significant differences from La are found in several samples for Rb, Ba, K_2O, U, Ta, Sr, and Nb.

Direct modeling has revealed that the composition of the Jingpohu volcanic rocks is partially similar to that of the Taryat volcanic rocks. The points for the Crater Forest basanites mostly align themselves along the line of melting from the mantle substratum with garnet concentration 5% at degrees of melting from 2–5%. The source of basaltoid mantle melts beneath the Jingpohu region was similar in composition to the source

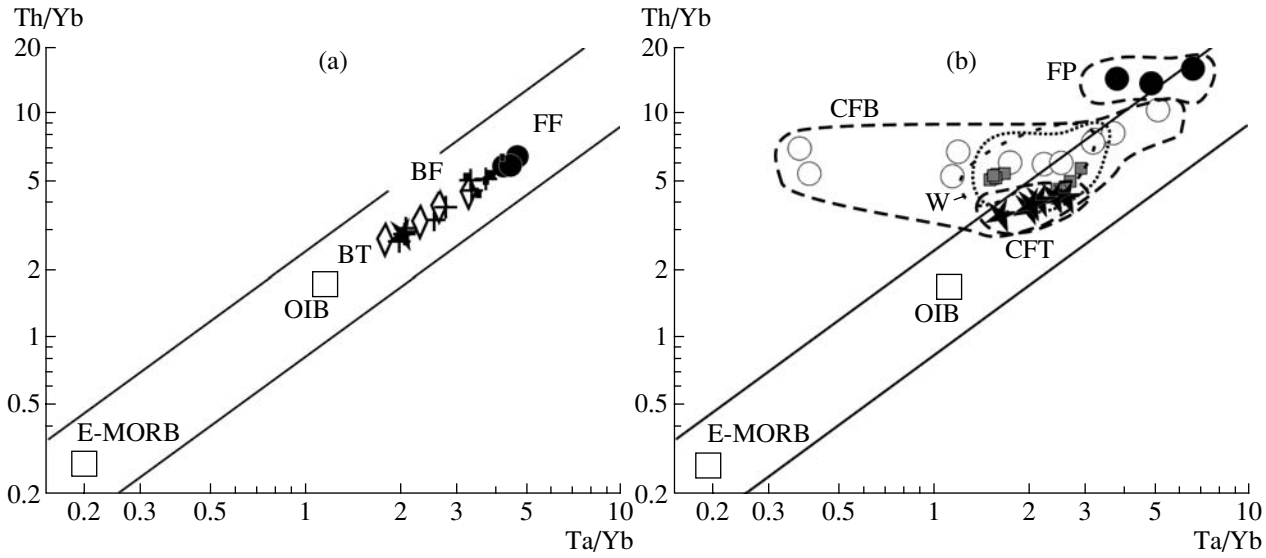

Fig. 7. The Th/Yb vs. Ta/Yb relationships in volcanic rocks of central Mongolia and Northeast China. For legend see Fig. 5. Straight lines enclose J. Pearce's mantle direction. Compositions of enriched basalts of mid-oceanic ridges (E-MORB) and oceanic island basalts (OIB) are plotted after [45].

beneath the Taryat Basin, but did not contain ilmenite. The Crater Forest trachybasalts formed by melting approximately 5% of the mantle source with 3% garnet, similarly to the basaltic trachyandesite from the Khorgo crater.

The distinctive feature of the Jingpohu melt source is the presence of rocks with low concentrations of ytterbium. These include the phonobasanite–phoidite group of the first and second cycles of activity at the Frog Pool volcanic center. Sample JP-2 from the Crater Forest line shows the lowest possible concentration of ytterbium (Table 2), that sample being typical of the third eruptive cycle at the Crater Forest line. Compositions such as these correspond to melts derived from a source having a garnet concentration of approximately 8%. According to the equilibrium melting model, partial mantle melts produced during the first eruptive cycle were approximately 2% beneath Frog Pool Volcano and approximately 5% beneath the Crater Forest line. During the second eruptive cycle, the degree of melting beneath Frog Pool remained the same, while varying between 2 and 5% beneath Crater Forest. During the third eruptive cycle, the melting beneath Crater Forest increased to reach 5%, with garnet concentrations between 8% at the source of JP-2 basanite and 3% at the source of trachybasalts (Fig. 9b).

A variation in garnet concentration between 5 and 8% is found at the source of the Wudalianchi Quaternary magma melts at melting degrees of 0.5 to 1.8%, according to the equilibrium model. One distinctive feature of the Laoheishan and Huoshaoshan volcanoes is the alignment of points along the line having a garnet concentration of approximately 5%.

Estimation of magma generation depth. A crude estimate of the depth of magma generation can be found from the composition of volcanic rocks and geophysical data.

The pressure that is correct for a given chemical composition is usually calculated from experimental data on the melting of "dry" mantle peridotites. Since compositions with Mg# = 70 or greater that are in equilibrium with mantle peridotites are not found in the volcanic complexes of central Mongolia and Northeast China studied here, the inference from this is that all basaltoid magmas were derived from metasomatized mantle sources, hence the available regression equations are not applicable to them.

Judging from the presence of garnet in the Taryat peridotite source, the depth of melting must be at least 80 km. Probable melting zones were identified in central Mongolia in the form of discrete low-velocity lenses in the depth interval between 70–80 to 120–140 km along a detailed seismic tomography profile (MOBAL-2003) derived from records of converted *SV* waves [20]. Such a lens may have served as a source of alkali basaltoids discharged onto the Taryat Basin. No liquids from garnetless mantle rocks are present in the ejecta from the Holocene volcanoes in this area. Magma generation beneath the Holocene volcanoes of Northeast China is estimated to occur at a depth of at least 80 km, from the presence of garnet in the source, and at a depth equal to or less than 120 km, based on determinations of lithosphere thickness by geophysical techniques [64].

The volcanic rocks in both areas under study show wide variations in Yb, due to changes in garnet abundances in the mantle sources. Mantle peridotites with

Table 2. Concentrations of major oxides (wt %), trace elements (ppm), and strontium isotope ratios in representative samples of Holocene volcanic rocks in the Jingpohu and Wudalianchi regions of Northeast China

Column number	1	2	3	4	5	6	7	8
Specimen number	DX1-26	DX4-28	JP-2	JP-3	91J03	HM5	HM3	HS2-2
SiO_2	46.18	44.25	47.52	47.70	48.40	47.40	47.80	48.90
TiO_2	1.80	1.85	1.72	1.70	1.39	1.94	1.90	2.24
Al_2O_3	15.02	14.66	15.15	15.08	15.03	17.13	17.19	13.00
Fe_2O_3	4.19	5.58	2.30	2.32	Not dtm.	3.71	4.18	9.64
FeO	6.81	5.30	8.53	8.46	11.20	6.63	6.16	Not dtm.
MnO	0.18	0.19	0.19	0.18	0.20	0.16	0.16	0.15
MgO	8.78	8.88	8.56	8.67	8.57	4.59	4.51	7.88
CaO	8.69	8.73	8.64	8.57	8.73	5.85	5.85	8.03
Na_2O	4.92	4.94	4.28	4.25	3.69	6.27	6.22	4.12
K_2O	2.32	3.11	2.25	2.19	2.04	4.74	4.79	4.73
P_2O_5	0.90	1.08	0.68	0.63	0.66	1.02	1.06	1.18
LOI	0.64	0.67	0.62	0.62	0.73	0.50	0.50	Not dtm.
Total	100.60	99.83	101.32	101.17	99.91	100.72	100.94	99.84
Sc	11.9	11.0	7.3	12.8	16.3	5.5	5.5	12.1
Cr	170	205	166	176	193	52	47	Not dtm.
Co	53	51	51	53	39	44	43	Not dtm.
Ni	118	263	111	117	59	34	39	Not dtm.
V	191	161	156	161	139	94	91	Not dtm.
Rb	41	53	37	39	Not dtm.	74	78	89
Sr	786	980	679	662	645	957	966	1735
Y	18.4	20.2	17.5	17.4	22.5	16.9	16.5	27.0
Zr	184	230	189	188	172	349	348	363
Nb	51	64	59	59	48.8	95	89	71
Cs	Not dtm.	Not dtm.	Not dtm.	Not dtm.	Not dtm.	Not dtm.	Not dtm.	0.82
Ba	520	610	588	586	642	635	605	1881
La	49.5	63.6	35.9	42.8	41.4	67.1	66.1	112
Ce	78.7	97.4	53.9	66.1	66.6	106	105	195
Pr	8.42	10.4	5.87	7.11	Not dtm.	11.4	11.4	21.8
Nd	31.4	39.2	21.7	26.8	33.2	42.7	41.9	80
Sm	7.19	8.48	4.84	6.01	5.98	9.2	8.8	13.9
Eu	2.11	2.49	1.48	1.86	2.15	2.56	2.52	3.75
Gd	6.12	6.28	4.07	5.07	Not dtm.	6.2	6.28	9.81
Tb	0.77	0.87	0.53	0.69	0.84	0.79	0.85	1.19
Dy	3.95	4.43	2.56	3.61	Not dtm.	4.05	3.95	5.64
Ho	0.72	0.73	0.46	0.68	Not dtm.	0.65	0.6	0.9
Er	1.48	1.53	0.85	1.38	Not dtm.	1.17	1.11	2.03
Tm	0.2	0.2	0.1	0.2	Not dtm.	0.2	0.2	0.2
Yb	1.26	1.3	0.78	1.27	1.61	0.88	0.84	1.31
Lu	0.17	0.19	0.12	0.18	0.3	0.13	0.12	0.18
Hf	3.5	4.5	4	4.3	4.05	7.8	7.4	8.33
Ta	Not dtm.	Not dtm.	4	Not dtm.	3.52	4.3	3.2	4.4
Pb	Not dtm.	Not dtm.	Not dtm.	Not dtm.	6.3	Not dtm.	Not dtm.	12
Th	6.9	9	8.1	8.2	6.64	12	12	8.2
U	1.7	2.4	1.8	1.9	1.69	3.1	3.2	1.63
$^{87}Sr/^{86}Sr$	0.703968 ± 13	0.704039 ± 26	0.704488 ± 15	0.704537 ± 18	Not dtm.	0.704288 ± 36	0.704294 ± 20	0.705054 ± 13

Table 2. (Contd.)

Column number	9	10	11	12	13	14	15	16
Specimen number	HN6-1	L-13	LE6-4	LW5-2	HK-2	92W10	H-38	A-4
SiO_2	51.13	53.89	50.97	51.08	50.37	49.02	48.16	52.79
TiO_2	2.25	2.32	2.28	2.53	2.22	2.33	2.29	2.30
Al_2O_3	13.53	13.95	13.22	13.20	13.37	12.92	12.95	13.81
Fe_2O_3	9.00	8.40	8.94	9.04	9.21	Not dtm.	9.76	8.21
FeO	Not dtm.	Not dtm.	Not dtm.	Not dtm.	Not dtm.	7.90	Not dtm.	Not dtm.
MnO	0.13	0.11	0.13	0.13	0.14	0.15	0.14	0.11
MgO	7.25	5.88	7.68	6.86	7.67	8.40	7.75	5.57
CaO	7.12	5.45	6.67	6.57	7.58	9.12	8.11	5.19
Na_2O	3.82	3.98	3.90	3.83	3.94	4.27	4.18	3.89
K_2O	4.51	5.43	4.90	5.39	4.45	4.85	4.59	5.43
P_2O_5	0.93	0.99	1.00	1.15	1.02	0.93	1.11	0.99
LOI	Not dtm.	−0.33	Not dtm.	Not dtm.	Not dtm.	0.07	−0.03	0.83
Total	99.64	98.65	99.66	99.75	99.97	99.89	99.01	99.12
Sc	13.1	13.0	13.4	13	Not dtm.	14.2	13.0	13
Cr	Not dtm.	167	Not dtm.	Not dtm.	Not dtm.	224	200	171
Co	Not dtm.	29	Not dtm.	Not dtm.	Not dtm.	35	Not dtm.	22
Ni	Not dtm.	174	Not dtm.	Not dtm.	Not dtm.	152	160	148
V	Not dtm.	Not dtm.	Not dtm.	Not dtm.	Not dtm.	129	Not dtm.	Not dtm.
Rb	85	102	92	100	Not dtm.	Not dtm.	89	100
Sr	1350	1420	1379	1479	Not dtm.	1084	1653	1353
Y	22.7	23.7	22.8	23.7	Not dtm.	33	26.5	23.1
Zr	344	544	396	444	Not dtm.	313	373	532
Nb	58	66	67	70	Not dtm.	57	72	66
Cs	0.76	Not dtm.	0.82	0.89	Not dtm.	Not dtm.	Not dtm.	Not dtm.
Ba	1558	1565	1600	1834	Not dtm.	1784	1912	1548
La	80.1	83	85.8	96.4	Not dtm.	94.1	99	82
Ce	142	159	151	171	Not dtm.	158	185	157
Pr	16.1	18	16.9	19.1	Not dtm.	Not dtm.	21	18
Nd	59.4	65	69.1	69.7	Not dtm.	73.4	78	66
Sm	10.7	11	11	12	Not dtm.	11.9	13	11
Eu	2.93	3	2.94	3.23	Not dtm.	3.6	3.7	3
Gd	7.84	8.2	7.94	8.62	Not dtm.	Not dtm.	10	7.8
Tb	0.97	1	0.97	1.04	Not dtm.	1.22	1	Not dtm.
Dy	4.64	4.6	4.7	4.9	Not dtm.	Not dtm.	5.6	4.6
Ho	0.75	1	0.76	0.8	Not dtm.	Not dtm.	1	0.9
Er	1.72	1.9	1.76	1.84	Not dtm.	Not dtm.	2.2	2
Tm	0.2	Not dtm.	0.2	0.2	Not dtm.	Not dtm.	Not dtm.	Not dtm.
Yb	1.23	1.3	1.2	1.24	Not dtm.	1.28	1.4	1.3
Lu	0.18	0.19	0.17	0.18	Not dtm.	0.2	0.2	0.18
Hf	8	13	9.09	10.3	Not dtm.	8.01	6.9	Not dtm.
Ta	3.6	3.2	4.2	4.4	Not dtm.	Not dtm.	4.1	Not dtm.
Pb	10.5	13	12	14	Not dtm.	13	12	16
Th	6.1	6	6.77	6.77	6.76	8.43	8	7
U	1.31	1.3	1.48	1.52	1.39	1.63	1.9	Not dtm.
$^{87}Sr/^{86}Sr$	0.705099 ± 11	0.705380 ± 10	0.705189 ± 11	0.705295 ± 11	0.705111 ± 11	Not dtm.	0.705070 ± 10	0.705410 ± 10

Note: 1–5 Crater Forest line, basanites (1–4) and trachybasalt (5), 6–7 phoidites from the Frog Pool volcanic center, 8–15 Laoheishan and Huoshaoshan volcanoes, Wudalianchi, Lh1 (8–13) and Lh2 (14, 15) phonobasanites, Lh1 trachyandesite (16). Data from [41, 52, 58, 61] were used. Not dtm. means Not determined.

Table 3. Partition coefficients for mineral/basic melt

Element	Ol [37]	Opx [37, 11]	Cpx [11, 33, 38, 39]	Grt [37, 11]	Phl [11, 33, 42, 43]	Ilm [56]	Ap [29, 42]
Rb	0.00002	0.0001	0.0047	0.00002	5.18	0.0004	0.01
Ba	0.000005	0.0001	0.0006	0.00002	3.48	0.0003	1.555
Th	0.000007	0.001	0.013	0.0012	0.0014	0.0005	2.131
U	0.000009	0.00023	0.006	0.0059	0.0028	0.0005	2.131
K	0.00002	0.0001	0.07	0.013	3.67		
Nb	0.00005	0.003	0.0027	0.002	0.0853	2.32	0.001
Ta	0.00005	0.005	0.012	0.008	0.1	1.7	0.001
La	0.0002	0.003	0.044	0.0007	0.0004	0.00003	7.39
Ce	0.00007	0.0021	0.084	0.0026	0.0006	0.00005	5.965
Pr	0.0003	0.0022	0.124	0.01	0.0009	0.0002	*4.64
Sr	0.00004	0.0015	0.096	0.0007	0.183	0.001	3.055
Zr	0.001	0.02	0.121	0.117	0.0232	0.3	0.012
Hf	0.0029	0.06	0.256	0.23	0.048	0.4	0.01
Sm	0.0009	0.0037	0.28	0.1	0.0008	0.0006	4.603
Ti	0.015	0.09	0.384	0.3	1.768	23	
Ho	0.01	0.019	0.38	2.5	0.0045	0.011	2.065
Y	0.0082	0.02	0.44	2.5	0.007	0.0045	3.43
Er	0.0109	0.021	0.35	3.3	0.0074	0.05	1.725
Yb	0.024	0.032	0.31	6.4	0.023	0.17	0.93
Lu	*0.026	0.042	0.27	7	0.029	0.09	0.75

Note: Ol olivine, Opx orthopyroxene, Cpx clinopyroxene, Grt garnet, Phl phlogopite, Ilm ilmenite, Ap apatite.
* Marks interpolated values.

large garnet concentrations are denser than those with lower ones, so that an increased role of garnet may reflect a general relative increase in source depth. Tectonic perturbation affecting mantle layers may produce portions of less dense material in a facies with increased garnet abundance that would be transported under the force of buoyancy into a facies with less garnet. In addition to liquids that are in equilibrium with the mantle facies with increased garnet abundance, liquids are also produced that are in equilibrium with a facies with lesser garnet abundance. Increased garnet abundance in liquids as time goes on reflects changing magma generation, passing from shallower to greater depths. Conversely, a decreased garnet abundance in liquids indicates a decreased depth of magma generation, probably proceeding as far as the depth of spinel mantle facies.

Increased garnet abundance in the source has been identified in a lava succession in the Khanui volcanic field of central Mongolia, where basaltic trachyandesites produced a large shield edifice during the time interval 4.2–3.7 Ma with the subsequent discharge of a small portion of high-alkali basanite–phonotephrite melts about 3.4 Ma. Our trace-element modeling of partial melting showed that the basaltic trachyandesites were derived from a source with 4.5% garnet, and that the basanite–phonotephrites were due to a source with 5–6% garnet. The first magma portion came from the upper depth of the magma-generating system and the second from the lower one [21].

Taking the abundance of garnet as a characteristic of the source depth in the mantle, we hypothesize a relative shallowing of melt depth during the evolution of magmatic processes beneath the Taryat volcanoes. The initial low (1.5–3.0%) melting at the mantle depth corresponding to 5% garnet was followed by stronger melting (up to 5%) at a shallower mantle depth corresponding to 3–5% garnet.

The magma source beneath the Crater Forest in Northeast China was located at the mantle depth possessing 3–5% garnet in the time interval of 5430–4400 BP. A deeper source, corresponding to 8% garnet, was found beneath the Frog Pool volcanic center at the beginning of this interval and beneath the Crater Forest at the end. Considered on the scale of the Quaternary evolution of Wudalianchi volcanism, the last magma portions on the Laoheishan and Huoshaoshan volcanoes were from a velatively shallow source. The eruptions at these volcanoes were due to a source that was comparable in garnet abundance with the mantle material of most liquids beneath the Crater Forest, and the preceding Quaternary Wudalianchi liquids came from

Table 4. Correlation coefficients R^2 between concentrations of lanthanum (C_{La}) and concentration ratios of an element to lanthanum (C_i/C_{La}) for volcanic rock samples of the Late Pleistocene–Holocene and Quaternary

Element *i* to be compared	R^2					
	Taryat Basin		Jingpohu region		Wudalianchi region	
	Khorgo Volcano and east–west line of volcanoes (24)	Quaternary volcanic rocks (26)	Crater Forest and Frog Pool (21)	Crater Forest (18)	Laoheishan and Huoshaoshan volcanoes, Holocene (28)	Quaternary volcanic rocks (15)
Rb	0.926	0.953	–0.137	0.471	0.864	0.966
Ba	0.902	0.941	0.921	0.904	0.293	0.532
Th	0.934	0.765	0.367	0.723	0.319	0.771
U	0.936	0.848	0.031	0.490	0.491	0.682
K_2O	0.895	0.962	–0.232	0.201	0.876	0.836
Nb	0.865	0.903	0.122	0.369	0.615	0.150
Ta	0.798	0.823	0.359	0.445	–0.174	0.820
Ce	0.617	0.825	0.359	0.412	0.109	0.648
Pr	0.875	0.825	0.154	0.252	0.621	–
Nd	0.892	0.830	0.608	0.610	0.530	0.468
Sm	0.904	0.791	0.741	0.740	0.321	0.903
Eu	0.946	0.921	0.834	0.794	0.355	0.916
Dy	0.976	0.935	0.827	0.793	0.694	–
Ho	0.988	0.955	0.808	0.811	0.609	–
Er	0.952	0.972	0.731	0.673	0.665	–
Yb	0.985	0.986	0.840	0.842	0.875	0.818
Lu	0.945	0.962	0.718	0.791	0.692	0.838
Sr	0.832	0.959	0.645	0.671	–0.100	0.726
Zr	0.802	0.969	0.128	0.803	0.537	0.018
Hf	0.911	0.943	0.310	0.715	0.690	0.767
TiO_2	0.994	0.994	0.895	0.867	0.642	0.912
Y	0.974	0.971	0.932	0.943	0.496	0.542
Sc	0.922	0.841	0.774	0.870	0.628	0.900
Cr	0.880	0.314	0.582	0.908	0.264	0.870
Co	0.967	0.960	0.777	0.674	0.120	0.894
Ni	0.792	0.829	0.538	0.128	0.408	0.939
V	0.948	0.977	0.751	0.867	0.475	0.940

Note: The number of analyses is enclosed in parentheses. Dashes denote absence of data.

the substratum that was the source of volcanic rocks for Frog Pool and the terminal Crater Forest eruptions.

The conditions for the evolution of Holocene volcanism in central Mongolia. The impact of the Indian indentor on Asia is imprinted in the Cenozoic tectonic deformation of the upper crust. According to earthquake source mechanism data, the present-day compression propagates from the India–Asia collision zone as far as the southwestern part of the Baikal Rift System [62]. Overthrusts have been identified there due to north–south crustal compression during Pliocene–Quaternary time [13].

Strong collision-caused compressive stresses seem to have been relieved in the lithosphere of central Mongolia and the southwestern Baikal Rift System in the form of short pulses. An analysis of volcanic episodes for the last 2 Ma revealed that the volcanic pulses in inner Asia and at the eastern and southern convergent interplate boundaries of Asia were not synchronized in the interval 2.0–1.5 Ma. This discrepancy was related to the absence of an appreciable influence of interplate processes on intraplate activity, and the synchronization of intraplate and interplate volcanic episodes that

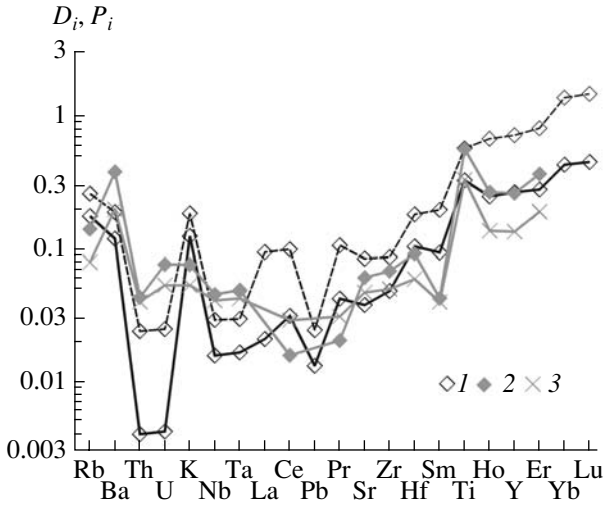

Fig. 8. Bulk partition coefficients D_i (continuous lines) and P_i (dashed lines) given by the modeling of partial melting based on rock compositions for the Taryat volcanoes: (*1*) direct equilibrium, (*2*) inverse equilibrium, and (*3*) direct fractional modeling

took place at approximately 1.2 Ma has been regarded as evidence for a stronger influence [17].

Melts of an isotopically rich magma source were discharged in the Taryat Basin at approximately 1.9 Ma ($^{87}Sr/^{86}Sr$ 0.7052–0.7053). The melts of the last 1.2 Ma had a lower level of $^{87}Sr/^{86}Sr$ 0.7046–0.7047, with wide variations in Sr abundance between 2000 and 625 ppm (Fig. 11). The increasing abundance of that element from the basaltic trachyandesite group through the basanite–phonobasanite group to the phonobasanite–phoidite group, with concurrently increasing $(La/Yb)_N$ (Fig. 9), emphasizes its role as an incompatible element that varies depending on the degree of partial melting at the mantle source. Identical values of $^{87}Sr/^{86}Sr$ at varying degrees of mantle rock melting reflected the homogeneity of the source material, which was melting without components of other mantle sources being involved.

The stable influence of the episodic effects of the collision-caused tectonic stress during the last 1.2 Ma has produced multiple eruptions in the Taryat Basin, in an east–west tectonic zone at least 80 km long. The Taryat Basin volcanism resulted from sinistral strike–slip displacements on an east–west magma-controlling fault.

The features in the evolution of basaltoid melts identified here are explained by the melting of a local mantle volume by the mechanism of syntectonic adiabatic decompression. Magma generation of this type is due to the intrinsic heat content of the system during movement of a high-temperature portion of mantle material to a shallower region [4]. The events beneath the Taryat Basin include melting of material in the strike–slip region, and afterwards in the region of concentrated extensional deformation. An east–west conduit discharged magma melts with low degrees of partial melt-

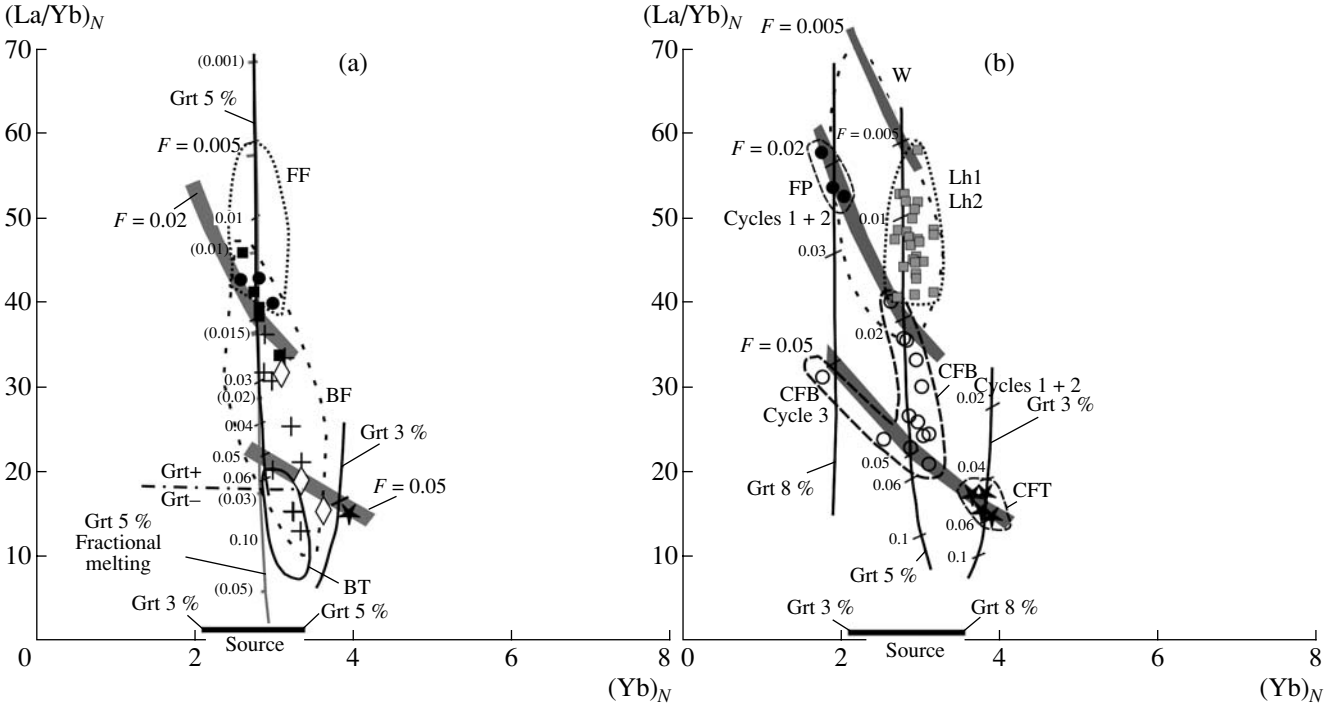

Fig. 9. The $(La/Yb)_N$ vs. Yb relationships for volcanic rocks of central Mongolia and Northeast China. For legend see Fig. 5. Shown are calculated lines of partial melting for sources with varying garnet abundances (for explanations see main text). The compositions have been normalized to undifferentiated mantle [45].

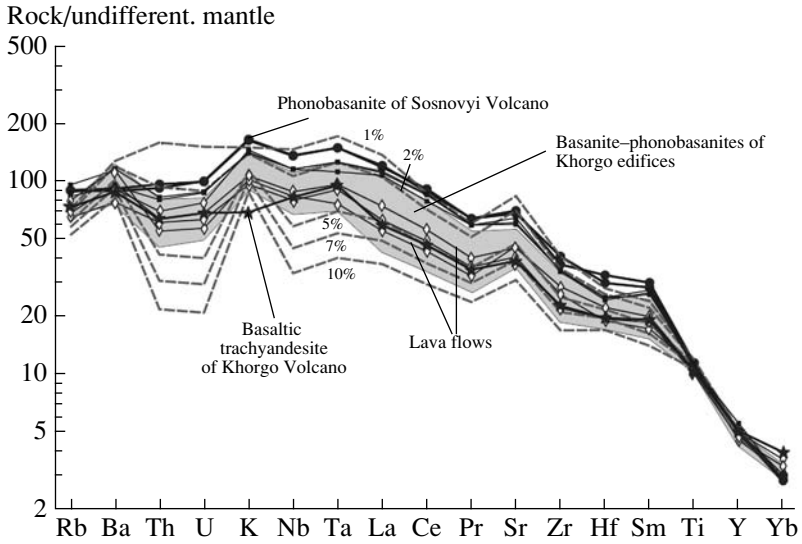

Fig. 10. Concentrations of incompatible trace elements in rocks of central Mongolia volcanoes and in melts derived from a hypothetical modeled source, based on equilibrium melting equations (1) (dashed lines without symbols). Numerals denote the degree of partial melting. For legend see Fig. 5. The compositions have been normalized to undifferentiated mantle [45].

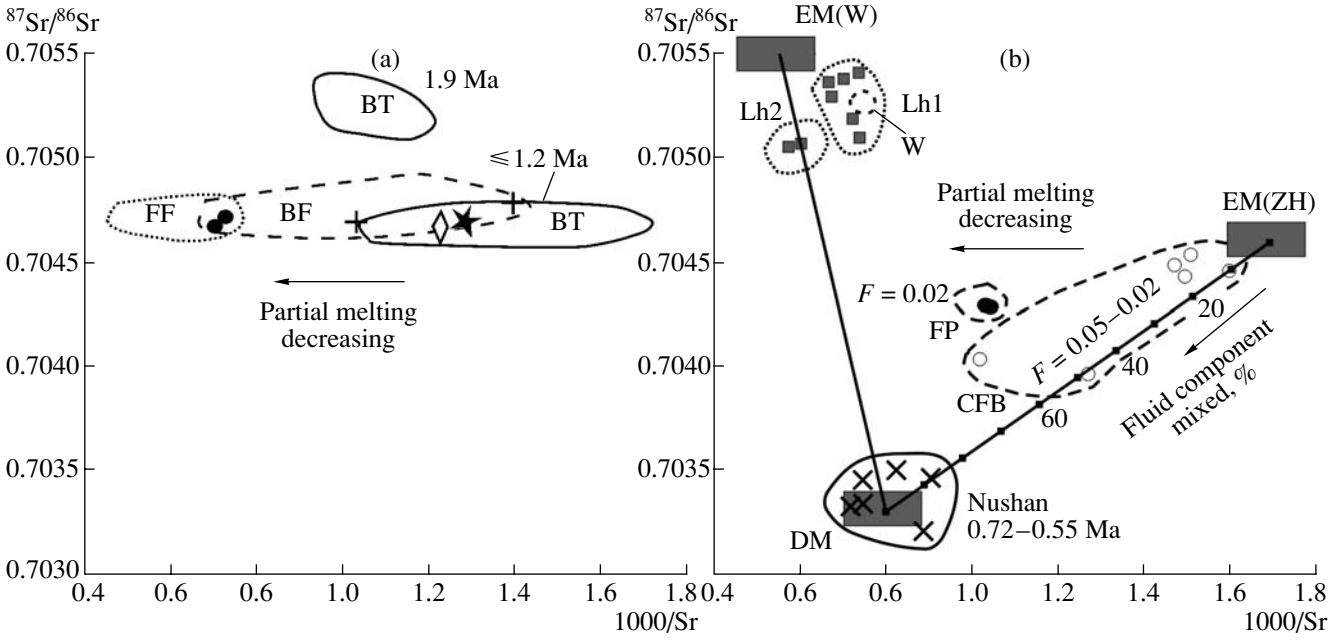

Fig. 11. The $^{87}Sr/^{86}Sr$ vs. 1000/Sr relationships for volcanic rocks of central Mongolia and Northeast China. For legend see Fig. 5. Panel a shows a basaltic trachyandesite field (BT), age 1.9 Ma. The decrease in 1000/Sr in volcanic rocks of age 1.2 Ma or younger is explained by the decrease in the degree of partial melting at the mantle source; panel b shows the following components: EM(ZH) slightly enriched Jingpohu mantle component, EM(W) strongly enriched Wudalianchi component, DM depleted component represented by Nushan basalts (compositions are shown by inclined crosses after [63]).

ing (1.5–3%) and the north–northeast conduit erupted melts of higher degrees (up to 5%) with lower garnet abundances at a shallower source (Fig. 12).

Conditions for the evolution of Holocene volcanism in Northeast China. The eastern margin of Asia was experiencing complicated Late Cenozoic changes in crustal stress and strain. The causes, character, and timing of these changes are a subject of debate [48]. The most important role in the dynamics of the continental margin was played by the north-northeast Tan-Lu fault (Tangcheng–Lujiang) fault (Fig. 3). The fault is thought to have experienced dextral movements during the Early/Middle Miocene, consistent with the general deformation pattern in Central and East Asia at the

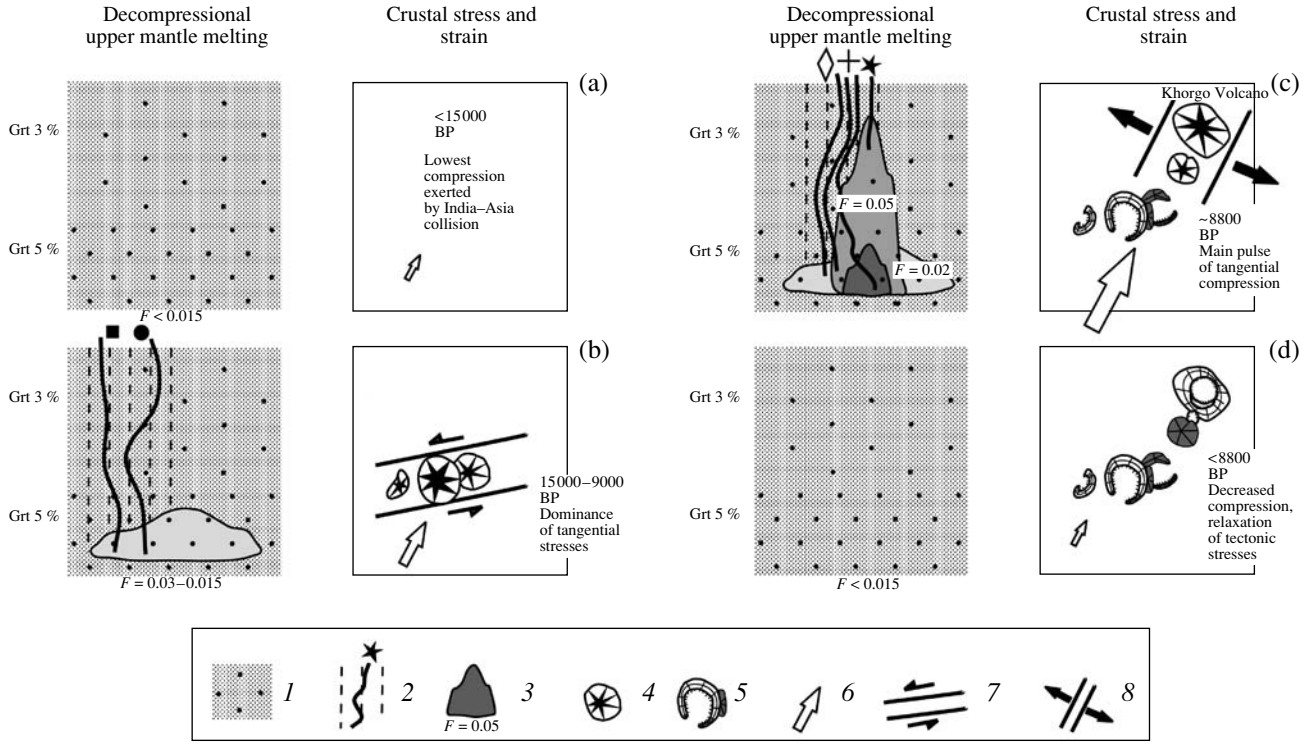

Fig. 12. Relation of decompressional mantle melting to volcanic evolution of Taryat Basin: (*1*) mantle rocks with garnet concentration varying between 3 and 5%, (*2*) magma conduits, for symbols denoting melt compositions see Figs. 2 and 5, (*3*) molten region with concentration of partial melt between 1.5 and 5% (the respective values of *F* calculated according to the partial melting model are 0.015 to 0.05), (*4*) active volcanoes, (*5*) edifices of extinct volcanoes (Fig. 2), (*6*) direction of pressure exerted by the India–Asia collision zone (greater arrows correspond to greater pressure), (*7*) strike–slip movement resulting from tangential stresses, (*8*) extension (tension combined with compression).

front of the India–Asia collision. The movement on the Tan-Lu fault was replaced at approximately 5–4 Ma by sinistral movement, because of compression at the collision front between the Izu–Bonin and Honshu arcs [16]. The movements were again replaced at approximately 2.4 Ma by dextral ones in connection with the increasing role of north–northeast compression emanating from the India–Asia collision zone [60]. The volcanic eruptions in Northeast Asia were caused by the last strong tectonic pulse. The fact that this volcanism occurred in antiphase with the Taryat volcanism needs an explanation. We think that this asynchronousness was due to the involvement of the fluid magma generation mechanism during the relaxation of tectonic stress in the lithosphere following the main tectonic pulse.

The Lh1 lava group of Laoheishan and Huoshaoshan volcanoes in the Wudalianchi region showed an appreciable excess of ^{230}Th relative to ^{238}U (^{230}Th/^{238}U = 1.24–1.33). The increase in ^{230}Th/^{232}Th, together with an increased abundance of K_2O and a higher ^{87}Sr/^{86}Sr ratio that also occurred simultaneously with lower ^{143}Nd/^{144}Nd and ^{206}Pb/^{204}Pb, provides evidence of the isotopic and element heterogeneity of the mantle source that appeared at approximately 350000 BP. The material of the garnet peridotite served as a component of the heterogeneous mixture, and metasomatic material served as another component. The isotope heterogeneity of basaltoid melts cannot have been due to mixing of magma material coming from sources of two isolated mantle regions, but formed by the transport of material into the peridotites involved in the melting [64].

Considerable inhomogeneity of the isotope composition of Sr, Nd, and Pb is generally typical of Quaternary volcanic rocks in East Asia. The most depleted lavas in the Nushan volcanic field, belonging to the age interval 0.72–0.55 Ma, were in agreement with the common sublithospheric component [63]. The erupted material in other volcanic fields and individual volcanoes consisted of mixtures of the common component and various lithospheric components.

In terms of trace element abundances, the Lh1 lava group of Laoheishan and Huoshaoshan volcanoes is comparable with the Quaternary Wudalianchi lavas, while the presence of the Lh2 group, that was not observed to have occurred prior to the 1720–1721 eruptions, shows that the magmatism was changing relative to the preceding magmatism of the Quaternary Period. Since the points do not show any significant displacement toward the depleted component of sublithospheric mantle (Fig. 11b), any relationship between the specific

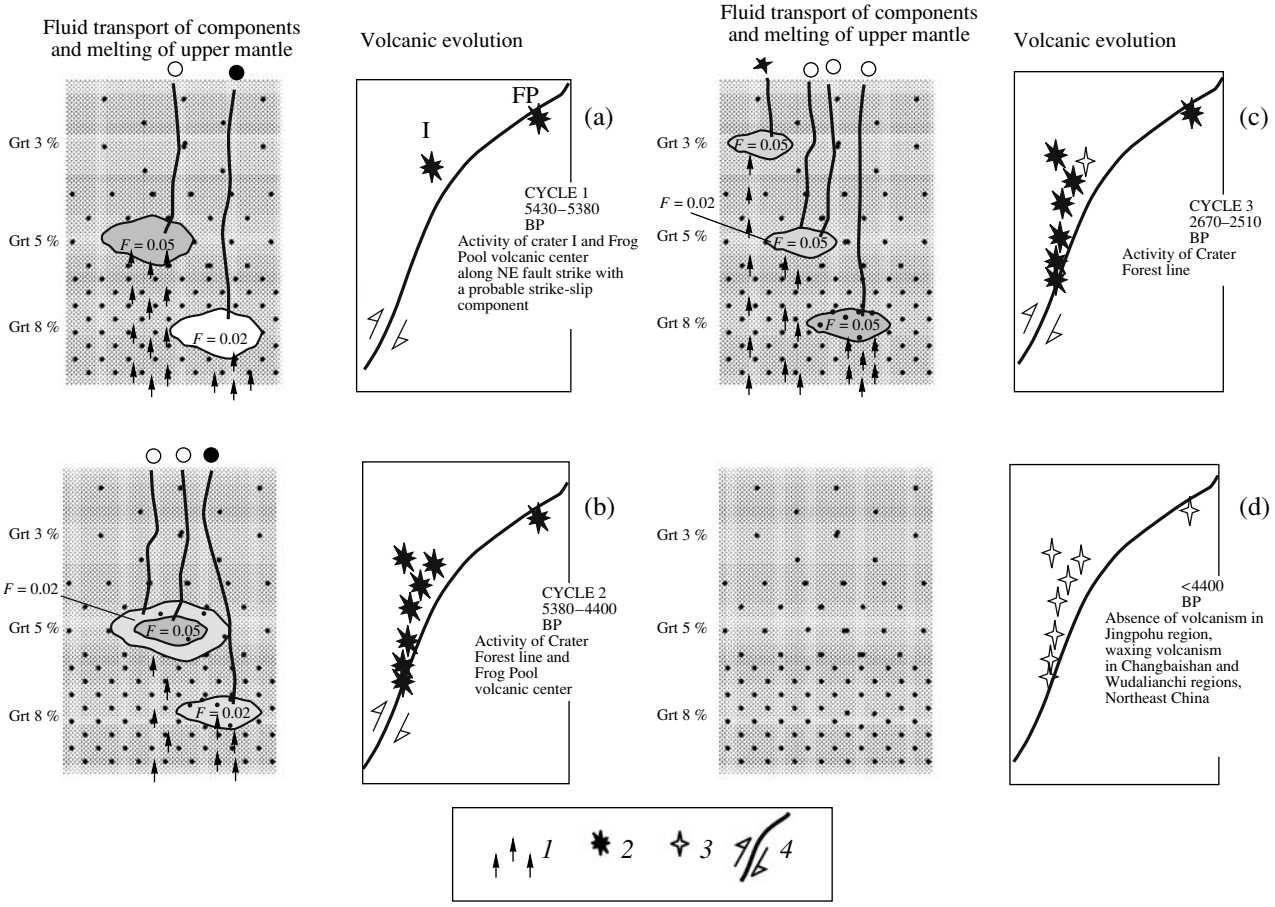

Fig. 13. Relation of fluid mantle melting to volcanic evolution in Jingpohu region, Northeast China: (*1*) transport of fluids from sublithospheric mantle upward to the depth of magma generation, (*2*) active volcano, (*3*) extinct volcano edifice, (*4*) fault showing episodic dextral strike–slip movement. For legend see Fig. 12.

composition of the Lh2 group and an increased supply of deeper material is ruled out. The relative decrease in the role of garnet (Fig. 9b) is interpreted in relation with the abundances of present-day alkali-basaltoid liquids in the upper part of the mantle magma generation zone.

Although the ejecta of volcanic eruptions at the Crater Forest line are similar in their composition and degree of melting at the mantle source with the ejecta at the Khorgo volcanic line, the similarity is far from being complete. The depletion in high field strength elements (Nb, Ta, Ti) shows that the Jingpohu alkali basaltoids were melted from the mantle material with the participation of aqueous fluids.

The isotope heterogeneity of the Jingpohu alkali basaltoids is clearly expressed in the $^{87}Sr/^{86}Sr$ vs. 1000/Sr coordinates (Fig. 11b). A slightly enriched and a depleted mantle component are distinguished. The former, similar to the mantle component of the Taryat Basin, is a metasomatized garnet peridotite; the latter, similar to the Nushan basalts, is material of the sublithospheric mantle. The points of compositions experiencing the greatest melting beneath the Crater Forest are rearranged between these components, while being displaced to the left of their mixing line with decreasing degree of melting. Considering that the Jingpohu volcanic rocks are depleted in high field strength elements, we suggest that the isotopically depleted component was brought into the peridotite by aqueous fluid. The Crater Forest rocks contain a 10 to 50% admixture of an isotope-depleted component, while the range for the Frog Pool volcanic center is 20–30%.

In contrast to the mechanism of adiabatic decompressional melting due to the intrinsic heat of the system, the fluid mechanism involving the heat supplied by deep-seated fluids and a decreased melting temperature of the mantle system [5] seems to favor longer support of magma generation.

CONCLUSION

(1) The timings of Holocene volcanic eruptions occurring in central Mongolia, northern Transbaikalia, and Northeast China were consistent among themselves. One common mechanism that could trigger volcanisms in regions so far apart could have been the impact of the last strong tectonic pulses propagating

from the India–Asia collision zone. The greatest tectonic stress found its expression in the structural rearrangement of the Udokan Range volcanic area of northern Transbaikalia at about 8780 BP. In the Taryat Basin of central Mongolia, eruptions at the east–west line of the Odnobokii, Listvennichnyi, and Sosnovyi volcanoes preceded the rearrangement, while the eruptions at the north-northeast line of Khorgo volcanic structures and the discharge of lava flows that flooded the area occurred either at the time of the rearrangement or immediately after it. The volcanism in Northeast China began simultaneously with the rearrangement of the Udokan volcanic area, with the greatest frequency of eruptions being reached 6000–8000 years after the rearrangement, i.e., during the last 2500–2200 years.

(2) The basanite–phonobasanite lava flows in the Taryat Basin are similar to the ejecta of the north–northeast Khorgo line in their trace element abundances. In addition to basanite–phonobasanites, phonobasanite–phoidites were found at the east–west volcanic line and basaltic trachyandesites were found in the main Khorgo volcanic cone. This compositional range is typical of volcanic rocks in the volcanoes of Northeast China (Jingpohu), which were active in the time interval 5430–4400 BP. The rocks from earlier eruptions at the line of the Odnobokii, Listvennichnyi, and Sosnovyi volcanoes are similar to those of earlier eruptions at the Frog Pool volcanic center, and the volcanic rocks at the later Khorgo volcanic line are similar to later rocks at Crater Forest. The ejecta of the 1720–1721 eruptions on the Laoheishan and Huoshaoshan volcanoes in the Wudalianchi region stand out sharply due to their potassium composition and other geochemical characteristics, which are generally typical of the Quaternary and Late Miocene lavas in the north–south zone of the Erkeshan, Wudalianchi, and Keluo volcanic fields.

(3) Metasomatized mantle garnet peridotites were the mantle sources of magma melts for the Holocene volcanoes in the Taryat Basin and Northeast China. Judging by the high correlation coefficients for incompatible elements, and by the homogeneous isotopic composition of strontium, the Taryat basaltoids were derived from a single mantle source that has been active since 1.2 Ma. The Holocene basaltoids of Northeast China are typically heterogeneous in incompatible trace elements and their $^{87}Sr/^{86}Sr$, $^{143}Nd/^{144}Nd$, and $^{206}Pb/^{204}Pb$ isotope ratios (including also $^{230}Th/^{238}U$ for the recently active Wudalianchi volcanoes).

(4) The rocks in Northeast China are different from those found in central Mongolia in being depleted in high field strength elements (Nb, Ta, Ti). It is therefore supposed that the Taryat isotopically homogeneous basaltoids were generated by the mechanism of adiabatic decompressional melting, while the isotope-heterogeneous ones in Northeast China were the result of deep-seated aqueous fluids being transported into the lower lithosphere. Accordingly, the decompressional mechanism was realized in small degrees of melting (1.5–3.0%), which occurred simultaneously with strike–slip movements, and that reached 5% at the time of the greatest tangential compression. The fluid-melting mechanism began to be felt only at the time of the greatest collision compression, and developed later. One such later episode in the Jingpohu region involved initial melting of approximately 2% beneath the Frog Pool volcanic center, along with increased partial melting and a subsequent overall increase in melting to 5% beneath the Crater Forest line.

ACKNOWLEDGMENTS

This work is being carried out under the integration projects of the Siberian Branch of the Russ. Acad. Sci. no. 7.10.3/2006 and DVO RAN no. 06-1-P16-065, the regional project of the Russian Foundation for Basic Research no. 05-05-97254-r-baikal, and presidential grant no. MK-10106.2006.5. The field work on the Taryat volcanoes was carried out with the participation of A.V. Ivanov.

REFERENCES

1. Genshaft, Yu.S. and Saltykovskii, A.Ya., *Katalog vklyuchenii glubinnykh porod i mineralov v bazal'takh Mongolii* (A Catalog of Inclusions Deriving from Deep-Seated Rocks and Minerals in Mongolian Basalts), Moscow: Nauka, 1990.
2. Devyatkin, E.V., The Geochronology of Mongolian Cenozoic Basalts and their Relation to Neotectonic Features, *Stratigrafiya. Geol. Korrelyatsiya*, 2004, vol. 12, no. 2, pp. 102–114.
3. Zonenshain, L.P. and Kuz'min, M.I., *Paleogeodinamika* (Paleogeodynamics), Moscow: Nauka, 1992.
4. Kadik, A.A. and Frenkel', M.Ya., *Dekompressiya porod kory i verkhnei mantii kak mekhanizm obrazovaniya magm* (Decompression of Crustal and Upper Mantle Rocks as a Mechanism of Magma Generation), Moscow: Nauka, 1982.
5. Kadik, A.A. and Lukanin, O.A., *Degazatsiya verkhnei mantii pri plavlenii* (Degassing of Upper Mantle during Melting), Moscow: Nauka, 1986.
6. *Karta geologicheskikh formatsii Mongol'skoi narodnoi respubliki. Scale 1 : 1500000* (A Map of Geologic Formations in the Mongolian People's Republic, Scale 1 : 1500000), Yanshin, A.L., Ed., Joint Soviet–Mongolian Scientific Expedition, 1989.
7. Kiselev, A.I., Cenozoic Volcanism in Central and East Asia, in *Problemy razlomnoi tektoniki* (Problems in Fault Tectonics), Novosibirsk: Nauka, 1981, pp. 71–86.
8. Kepezhinskas, V.V., Devyatkin, E.V., and Dashdavaa, Z., Cenozic Basalts of the Taryat Depression, *Geologiya i Geofizika*, 1975, no. 4, pp. 3–14.
9. Kononova,V.A., Ivanenko, V.V., Karpenko, M.I., et al., New Evidence Relating to the K–Ar Age of Cenozoic Continental Basalts in the Baikal Rift System, *Dokl. AN SSSR*, 1988, vol. 303, no. 2, pp. 454–457.
10. Kudryashova, E.A., Yarmolyuk, V.V., Lebedev, V.A., et al., Geochronology and Patterns of Volcanism Migra-

tion in the Khangai Late Cenozoic Volcanic Area, in *Izotopnoe datirovanie protsessov rudoobrazovaniya, magmatizma. Mater. III Rossiiskoi konf. po izotopnoi geokhronologii* (Isotope Dating of Mineralization and Magmatism. Proc. III Russian Conf. on Isotope Geochronology), Moscow: GEOS, 2006, vol. 1, pp. 355–362.

11. Litasov, K.D., *Geochemical Models for the Evolution of Mantle Magmatic Systems Based on a Study of Deep-Seated Xenoliths, Eastern Transbaikalia*, Extended Abstract of Cand. Sci. (Geol.–Mineral.) Dissertation, Novosibirsk, 1998.
12. Logachev, N.A., Devyatkin, E.V., Malaeva, E.M., et al., Cenozoic Deposits in the Taryat Basin and in the Chulutu R. Valley, Central Khangai, *Izv. AN SSSR. Ser. Geol.*, 1982, no. 8, pp. 76–86.
13. Rasskazov, S.V., A Pliocene–Quaternary Overthrust in the Southern Okinskii Plateau, Eastern Sayany, *Geologiya i Geofizika,* 1990, no. 5, pp. 134–138.
14. Rasskazov, S.V., Hotspot Volcanism and the Structure of the Western Baikal Rift System, *Geologiya i Geofizika*, 1991, no. 9, pp. 72–81.
15. Rasskazov, S.V., Middle Holocene Variation of Tectonic Stress in the Volcanic Udokan Range Zone, Eastern Siberia, *Vulkanol. Seismol.*, 1999, no. 2, pp. 70–74.
16. Rasskazov, S.V., Logachev, N.A., and Ivanov, A.V., Correlation of Late Cenozoic Tectonic and Magmatic Events in the Baikal Rift System with Events in the Southeast of the Eurasian Plate, *Geotektonika*, 1998, no. 4, pp. 25–40.
17. Rasskazov, S.V., Logachev, N.A., Brandt, I.S., et al., *Geokhronologiya i geodinamika pozdnego kainozoya (Yuzhnaya Sibir'—Yuzhnaya i Vostochnaya Aziya)* (Late Cenozoic Geochronology and Geodynamics: Southern Siberia to South and East Asia), Novosibirsk: VO Nauka, 2000.
18. Rasskazov, S.V., Logachev, N.A., Kozhevnikov, V.M., et al., Stage Dynamics in the Upper Mantle of East Asia: Relationships between Migrating Volcanism and Low-Velocity Anomalies, *Dokl. RAN*, 2003, vol. 390, no. 1, pp. 90–95.
19. Rasskazov, S.V., Brandt, S.B., Brandt, I.S., et al., *Radioizotopnaya geologiya v zadachakh i primerakh* (Radio Isotope Geology in Problems and Examples), Novosibirsk: GEO, 2005.
20. Rasskazov, S.V., Mordvinova, V.V., Chuvashova, I.S., et al., Cenozoic Volcanism of Mantle Local Low-Velocity Anomalies in Central Mongolia and Southwestern Baikal Area, in *Vulkanizm i geodinamika: Mater. II Vserossiiskogo simpoziuma po vulkanologii i paleovulkanologii* (Volcanism and Geodynamics. Proc. III All-Russian Symp. on Volcanology and Paleovolcanology), Ulan-Ude: Izd-vo Buryatskogo nauchnogo tsentra, 2006, vol. 1, pp. 280–283.
21. Rasskazov, S.V., Yasnygina, T.A., Chuvashova, I.S., et al., The Dynamics of Mantle Melting beneath Central Mongolia during the Last 4 Myr: Relationships between Rare Earths in Lavas of the Khanui Volcanic Field, in *Tr. VI Rossiisko-Mongol'skoi konferentsii po astronomii i geofizike* (Proc. VI Russian–Mongolian Conf. on Astronomy and Geophysics), Irkutsk: In-t Zemnoi Kory SO RAN, 2006, pp. 150–164.
22. Romanovskii, N.P., *Tikhookeanskii segment Zemli: glubinnoe stroenie, granitoidnye rudno-magmaticheskie sistemy* (The Pacific Segment of the Earth: Deep Structure, Granitoid Ore–Magma Systems), Khabarovsk: ITiG DVO RAN, 1999.
23. Florensov, N.A., Solonenko, V.P., and Logachev, N.A., The Cenozoic Volcanism of Rift Zones, in *Vulkanizm i tektogenez* (Volcanism and Tectogenesis), Moscow: Nauka, 1968, pp. 146–151.
24. Chuvashova, I.S., Rasskazov, S.V., Brandt, I.S., et al., An Isotope Geochemical Characterization of Different-Aged Late Cenozoic Volcanic Rocks in the Taryat Basin, Central Mongolia, in *Izotopnoe datirovanie protsessov rudoobrazovaniya, magmatizma, osadkonakopleniya i metamorfizma. Mater. III Rossiiskoi konferentsii po izotopnoi geokhronologii* (Isotope Dating of Mineralization, Magmatism, Sedimentation, and Metamorphism. Proc. III Russian Conf. on Isotope Geochronology), Moscow: GEOS, 2006, vol. 2, pp. 401–405.
25. Yasnygina, T.A., Rasskazov, S.V., Markova, M.E., et al., Microelement Determination by ICP–MS Using Microwave Acid Decomposition in Basic and Intermediate Volcanic Rocks, in *Prikladnaya geokhimiya* (Applied Geochemistry), Moscow: IMGRE, 2003, no. 4, pp. 48–56.
26. Yarmolyuk, V.V., Kovalenko, V.I., and Bogatikov, O.A., The Southern Baikal Mantle Hotspot and its Role in the Generation of the Baikal Rift Region, *Dokl. AN SSSR*, 1990, vol. 312, no. 1, pp. 187–191.
27. Barry, T.L. and Kent, R.W., Cenozoic Magmatism in Mongolia and the Origin of Central and East Asian Basalts, in *Mantle Dynamics and Plate Interactions in Asia. Geodynamics*, 1998, vol. 27, pp. 347–364.
28. Barry, T.L., Saunders, A.D., Kempton, P.D., et al., Petrogenesis of Cenozoic Basalts from Mongolia: Evidence for the Role of Asthenospheric versus Metasomatized Lithospheric Mantle Sources, *J. Petrol.*, 2003, vol. 44, no. 1, pp. 55–91.
29. Chazot, G., Menzies, M.A., and Harte, B., Determination of Partition Coefficients between Apatite, Clinopyroxene, Amphibole, and Melt in Natural Spinel Iherzolites from Yemen: Implications for Wet Melting of the Lithospheric Mantle, *Geochim. Cosmochim. Acta*, 1996, vol. 60, pp. 423–437.
30. Class, C. and Goldstein, S.L., Plume–Lithosphere Interactions in the Ocean Basins: Constraints from the Source Mineralogy, *Earth Planet. Sci. Lett.*, 1997, vol. 150, pp. 245–260.
31. England, P. and Molnar, P., Active Deformation of Asia: From Kinematics to Dynamics, *Science*, 1997, vol. 278, pp. 647–650.
32. Enkhtuvshin, H., A Petrological Study on the late Mesozoic and Cenozoic Volcanic Rocks of the Mongolian Plateau, Master Thesis, Shimane University, 1995.
33. Foley, S.F., Jackson, S.E., Fryer, B.J., et al., Trace Element Partition Coefficients for Clinopyroxene and Phlogopite in an Alkaline Lamprophyre from Newfoundland by LAM–ICP–MS, *Geochim. Cosmochim. Acta*, 1996, vol. 60, pp. 629–638.
34. Fukao, Y., Obayashi, M., Inoue, H., et al., Subducting Slabs Stagnant in the Mantle Transition Zone, *J. Geophys. Res.*, 1992, vol. 97, pp. 4809–4822.

35. Gregoire, M., Moine, B.N., O'Reilly, S.Y., et al., Trace Element Residence and Partitioning in Mantle Xenoliths Metasomatized by Highly Alkaline, Silicate- and Carbonate-Rich Melts (Kerguelen Islands, Indian Ocean), *J. Petrol.*, 2000, vol. 41, pp. 477–509.
36. Gudmundsson, O. and Sambridge, M., A Regionalized Upper mantle (RUM) Seismic Model, *J. Geophys. Res.*, 1998, vol. 104, pp. 28803–28812.
37. Halliday, A.N., Lee, D.-C., Tommasini, S., et al., Incompatible Trace Elements in OIB and MORB and Source Enrichment in the Suboceanic Mantle, *Earth Planet. Sci. Lett.*, 1995, vol. 133, pp. 379–395.
38. Hart, S.R. and Dunn, T., Experimental cpx/Melt Partitioning of 24 Trace Elements, *Contrib. Miner. Petrol.*, 1993, vol. 113, pp. 1–8.
39. Hauri, E.H., Wagner, T.P., and Grove, T.L., Experimental and Natural Partitioning of Th, U, Pb and Other Trace Elements between Garnet, Clinopyroxene and Basaltic Melts, *Chem. Geol.*, 1994, vol. 117, pp. 149–166.
40. Hofmann, A.W. and Feigenson, M.D., Case Studies of the Origin of Basalt. I. Theory and Reassessment of Grenada Basalts, *Contrib. Mineral. Petrol.*, 1983, vol. 84, pp. 382–389.
41. Hsu, C.-H. and Chen, J-C., Geochemistry of Late Cenozoic Basalts from Wudalianchi and Jingpohu Areas, Heilongiang Province, Northeast China, *J. Asian Earth Sci.*, 1998, vol. 16, no. 4, pp. 385–405.
42. Ionov, D.A., Griffin, W.L., and O'Reilly, S.Y., Volatile-Bearing Minerals and Lithophile Trace Elements in the Upper Mantle, *Chem. Geol.*, 1997, vol. 141, pp. 153–184.
43. LaTourrette, T., Hervig, R.L., and Holloway, J.R., Trace Element Partitioning between Amphibole, Phlogopite and Basanite Melt, *Earth Planet. Sci. Lett.*, 1995, vol. 135, pp. 13–30.
44. Liu, J. and Taniguchi, H., Active Volcanoes in China, *Northeast Asian Studies*, 2001, vol. 6, pp. 173–189.
45. McDonough, W.F. and Sun, S.-S., The Composition of the Earth, *Chemical Geology*, 1995, vol. 120, pp. 223–253.
46. Nakamura, E., Campbell, I.H., and McCulloch, M.T., Chemical Geodynamics in a Back Arc Region around the Sea of Japan: Implications for the Genesis of Alkaline Basalts in Japan, Korea, and China, *J. Geophys. Res.*, 1989, vol. 94, pp. 4634–4654.
47. O'Reilly, S.Y. and Griffin, W.L., Apatite in the Mantle: Implications for Metasomatic Processes and High Heat Production in Phanerozoic Mantle, *Lithos*, 2000, vol. 53, pp. 217–232.
48. Rasskazov, S., Taniguchi, H., Goto, A., et al., Magmatic Expression of Plate Subduction beneath East Asia in the Mesozoic through Cenozoic, *Northeast Asian Studies*, 2004, vol. 9, pp. 179–219.
49. Reimer, P.J., Baillie, M.G.L., Bard, E., et al., IntCal04 Terrestrial Radiocarbon Age Calibration, 0–26 Cal Kyr BP, *Radiocarbon*, 2004, vol. 46, no. 3, pp. 1029–1058.
50. Seno, T., Syntheses of the Regional Stress Fields of the Japanese Islands, *The Island Arc*, 1999, vol. 8, pp. 66–79.
51. Shaw, D.M., Trace Element Fractionation during Anatexis, *Geochim. Cosmochim. Acta*, 1970, vol. 34, pp. 237–243.
52. Wang, Y., Mu, L., and Liu, W., Regularity and Characteristic of Volcanic Activity at Wudalianchi, Heilongjiang, in *Proc. 30th Intern. Geol. Congr.*, Beijing, China, 1996.
53. Williams, H.M., Turner, S.P., Pearce, J.A., et al., Nature of the Source Regions for Postcollisional, Potassic Magmatism in Southern and Northern Tibet from Geochemical Variations and Inverse Trace Element Modeling, *J. Petrol.*, 2004, vol. 45, pp. 555–607.
54. Windley, B.F. and Allen, M.B., Mongolian Plateau: Evidence for a Late Cenozoic Mantle Plume under Central Asia, *Geology*, 1993, vol. 21, pp. 295–298.
55. Yanovskaya, T.B. and Kozhevnikov, V.M., 3D *S*-Wave Velocity Pattern in the Upper Mantle beneath the Continent of Asia from Rayleigh Wave Data, *Phys. Earth Planet. Inter.*, 2003, vol. 138, pp. 263–278.
56. Zack, T. and Brumm, R., Ilmenite–Liquid Partition Coefficient of 26 Trace Elements Determined through Ilmenite/Clinopyroxene Partitioning in Garnet Pyroxenites, *Ext. Abst. VII Int. Kimb. Conf. Care Town, South Africa*, 1998, pp. 986–988.
57. Zhang, C.L., The Characteristics of Cenozoic Distribution in Jilin Province, in *30th Intern. Geol. Congr.*, Beijing, China, 1996.
58. Zhang, M., Suddaby, P., Thompson, R.N., et al., Potassic Rocks in NE China: Geochemical Constraints on Mantle Source and Magma Genesis, *J. Petrology*, 1995, vol. 36, no. 5, pp. 1275–1303.
59. Zhang, Y., Quaternary Volcanic Activity in China, in *The Quaternary of China*, Beijing: Science Press, 1991, pp. 274–306.
60. Zhang, Y., Shi, W., and Dong, S., Cenozoic Deformation History of the Tangcheng–Lujiang Fault Zone, North China, and Dynamic Implications, *The Island Arc*, 2003, vol. 12, pp. 281–293.
61. Zhang, Z., Feng, C., Li, Z., et al., Petrochemical Study of the Jingpohu Holocene Alkali Basaltic Rocks, Northeastern China, *Geochem. J.*, 2002, vol. 36, pp. 133–153.
62. Zoback, M.L., First- and Second-Order Patterns of Stress in the Lithosphere: The World Stress Map Project, *J. Geophys. Res.*, 1992, vol. 97, no. B8, pp. 11703–11728.
63. Zou, H., Zindler, A., Xu, X., et al., Major, Trace Element, and Nd, Sr, and Pb Isotope Studies of Cenozoic Basalts in SE China: Mantle Sources, Regional Variations, and Tectonic Significance, *Chem. Geol.*, 2000, vol. 171, pp. 33–47.
64. Zou, H., Reid, M.R., Liu, Y., et al., Constraints on the Origin of Historic Potassic Basalts from Northeast China by U–Th Disequilibrium Data, *Chem. Geol.*, 2003, vol. 200, pp. 189–201.